2015

Contribution of a mutational hot spot to hemoglobin adaptation in high-altitude Andean house wrens

Spencer C. Galen
University of New Mexico, Albuquerque

Chandrasekhar Natarajan
University of Nebraska-Lincoln, chandrasekhar.natarajan@unl.edu

Hideaki Moriyama
University of Nebraska-Lincoln, hmoriyama2@unl.edu

Roy E. Weber
Aarhus University, Aarhus

Angela Fago
Aarhus University

See next page for additional authors

Contribution of a mutational hot spot to hemoglobin adaptation in high-altitude Andean house wrens

Spencer C. Galen[a,b,1], Chandrasekhar Natarajan[c,1], Hideaki Moriyama[c], Roy E. Weber[d], Angela Fago[d], Phred M. Benham[e,2], Andrea N. Chavez[a,b], Zachary A. Cheviron[e,2], Jay F. Storz[c,3,4], and Christopher C. Witt[a,b,3,4]

[a]Department of Biology, University of New Mexico, Albuquerque, NM 87131; [b]Museum of Southwestern Biology, University of New Mexico, Albuquerque, NM 87131; [c]School of Biological Sciences, University of Nebraska, Lincoln, NE 68588; [d]Department of Bioscience, Zoophysiology, Aarhus University, DK-8000 Aarhus, Denmark; and [e]Department of Animal Biology, School of Integrative Biology, University of Illinois, Urbana–Champaign, IL 61801

Edited by Cynthia M. Beall, Case Western Reserve University, Cleveland, OH, and approved September 10, 2015 (received for review April 14, 2015)

A key question in evolutionary genetics is why certain mutations or certain types of mutation make disproportionate contributions to adaptive phenotypic evolution. In principle, the preferential fixation of particular mutations could stem directly from variation in the underlying rate of mutation to function-altering alleles. However, the influence of mutation bias on the genetic architecture of phenotypic evolution is difficult to evaluate because data on rates of mutation to function-altering alleles are seldom available. Here, we report the discovery that a single point mutation at a highly mutable site in the β^A-globin gene has contributed to an evolutionary change in hemoglobin (Hb) function in high-altitude Andean house wrens (*Troglodytes aedon*). Results of experiments on native Hb variants and engineered, recombinant Hb mutants demonstrate that a nonsynonymous mutation at a CpG dinucleotide in the β^A-globin gene is responsible for an evolved difference in Hb–O_2 affinity between high- and low-altitude house wren populations. Moreover, patterns of genomic differentiation between high- and low-altitude populations suggest that altitudinal differentiation in allele frequencies at the causal amino acid polymorphism reflects a history of spatially varying selection. The experimental results highlight the influence of mutation rate on the genetic basis of phenotypic evolution by demonstrating that a large-effect allele at a highly mutable CpG site has promoted physiological differentiation in blood O_2 transport capacity between house wren populations that are native to different elevations.

biochemical adaptation | hemoglobin | high altitude | hypoxia | mutation bias

An important question in evolutionary genetics is whether certain mutations or certain types of mutation make disproportionate contributions to phenotypic evolution (1–6). Within a given gene, the mutations that contribute to evolutionary changes in phenotype may represent a biased, nonrandom subset of all possible mutations that are capable of producing the same functional effect. The preferential fixation of particular mutations (substitution bias) could have several causes. Most theoretical and empirical attention has focused on causes of fixation bias, i.e., mutations have different probabilities of being fixed once they arise, due to differences in dominance coefficients or the magnitude of deleterious pleiotropy (1, 2, 4, 7–9). In principle, substitution bias can also stem directly from mutation bias (some sites have higher rates of mutation to alleles that produce the change in phenotype) (4, 9–11). However, empirical evidence for the importance of mutation bias is scarce for an obvious reason: even in rare cases where it is possible to document the contributions of individual point mutations to evolutionary changes in phenotype, data on rates of mutation to function-altering alleles are typically lacking. Rare exceptions include cases where loss-of-function deletion mutations can be traced to hot spots of chromosomal instability or highly mutable changes in the copy number of repetitive elements (12). Documenting cases where genetic changes at highly mutable loci contribute to phenotypic divergence is therefore important for elucidating the evolutionary significance of mutation bias. This is especially true for cases where mutations cause fine-tuned modifications of protein activity rather than simple losses of function.

Here, we report the discovery that a single amino acid replacement at a mutational hot spot in the avian β^A-globin gene has contributed to an evolutionary change in hemoglobin (Hb) function that has likely adaptive significance. By conducting experiments on native Hb variants and engineered recombinant Hb mutants, we demonstrate that a nonsynonymous mutation at a CpG dinucleotide in the β^A-globin gene of Andean house wrens (*Troglodytes aedon*) has contributed to an evolved difference in Hb–O_2 affinity between high- and low-altitude populations. In mammalian genomes, point mutations at CpG sites occur at a rate that is over an order of magnitude higher than the average for all other nucleotide sites (13, 14), and available data suggest a similar discrepancy in avian genomes (15, 16).

Andean house wrens are compelling subjects for studies of Hb function because this passerine bird species has an exceptionally broad and continuous elevational distribution, ranging from sea level to elevations >4,500 m (17). At 4,500-m elevation, the standard barometric pressure is ∼450 torr, so O_2 partial pressure (PO_2) is <60% that at sea level (∼96 torr compared to ∼160 torr).

Significance

Within a given gene, there may be many possible mutations that are capable of producing a particular change in phenotype. However, if some sites have especially high rates of mutation to function-altering alleles, then such mutations may make disproportionate contributions to phenotypic evolution. We report the discovery that a point mutation at a highly mutable site in the β-globin gene of Andean house wrens has produced a physiologically important change in the oxygenation properties of hemoglobin (Hb). The mutant allele that confers an increased Hb–O_2 affinity is present at an unusually high frequency at high altitude. These findings suggest that site-specific variation in mutation rate may exert a strong influence on the genetic basis of phenotypic evolution.

Author contributions: S.C.G., J.F.S., and C.C.W. designed research; S.C.G., C.N., H.M., P.M.B., and A.N.C. performed research; H.M., R.E.W., A.F., Z.A.C., J.F.S., and C.C.W. contributed new reagents/analytic tools; S.C.G., A.F., Z.A.C., J.F.S., and C.C.W. analyzed data; and J.F.S. and C.C.W. wrote the paper.

The authors declare no conflict of interest.

This article is a PNAS Direct Submission.

Data deposition: The newly generated sequences reported in this paper have been deposited in the GenBank database (accession nos. KT759682–KT760400). The parsed Illumina reads reported in this paper have been deposited in the National Center for Biotechnology Information (NCBI) Sequence Read Archive (SRA), www.ncbi.nlm.nih.gov/sra (PRJNA295865).

See Commentary on page 13753.

[1]S.C.G. and C.N. contributed equally to this work.

[2]Present address: Division of Biological Sciences, University of Montana, Missoula, MT 59812.

[3]J.F.S. and C.C.W. contributed equally to this work.

[4]To whom correspondence may be addressed. Email: jstorz2@unl.edu or cwitt@unm.edu.

This article contains supporting information online at www.pnas.org/lookup/suppl/doi:10.1073/pnas.1507300112/-/DCSupplemental.

Under such conditions, enhancements of pulmonary O_2 uptake and blood O_2 transport capacity are required to sustain O_2 flux to the tissue mitochondria in support of aerobic ATP synthesis (18). To complement changes in the cardiorespiratory system and microcirculation, changes in the O_2-binding affinity and cooperativity of Hb can enhance the O_2 capacitance of the blood (the total amount of O_2 unloaded for a given arteriovenous difference in O_2 tension). Because the optimal Hb–O_2 affinity is expected to vary according to the ambient PO_2, genetic variation in oxygenation properties of Hb may be subject to spatially varying selection between populations that inhabit different elevations. House wrens colonized South America in the late Pliocene or early Pleistocene via the newly formed Panamanian land bridge (19, 20), so the species may have been resident in the Andean highlands for up to ∼3 million years.

The Hb tetramer is composed of two semirigid $\alpha_1\beta_1$ and $\alpha_2\beta_2$ dimers that undergo a mutual rotation during the oxygenation-linked transition in quaternary structure between the deoxy (low-affinity "T") conformation and the oxy (high-affinity "R") conformation (21). This oxygenation-linked structural transition between the T and R states is the basis for cooperative O_2 binding, and is central to the allosteric function of Hb as an O_2 transport molecule. Our analysis of house wren Hb highlights the influence of mutation rate on the genetic basis of phenotypic divergence by demonstrating that mutation at a CpG dinucleotide produced a large-effect amino acid replacement at an $\alpha_1\beta_1$ intradimer contact (β55Val→Ile)—a replacement that produced a significant increase in Hb–O_2 affinity.

Results

We performed an integrative analysis of Hb polymorphism in Andean house wrens that combined a population genomic analysis of nucleotide variation with mechanistic studies of protein function. Our survey of Hb polymorphism in *T. aedon* was based on a total of 140 museum-vouchered specimens (Table S1) that we collected from a broad range of elevations in the Peruvian Andes (Fig. S1). Andean house wrens are characterized by a high degree of phylogeographic structure. In Peru alone, house wrens are divided into seven highly divergent mtDNA clades that have allopatric or parapatric distributions across the Andes (20). To minimize the confounding effects of population structure in our altitudinal survey of Hb polymorphism, we conducted a detailed population genetic analysis on a sample of 65 specimens from the western slope of the Andes in central Peru that are representatives of the same mtDNA clade (20). Comparisons between highland and lowland population samples were based on specimens collected from >3,000 and <1,000 m, respectively.

Hb Isoform Composition of Red Blood Cells. Most birds express two structurally distinct Hb isoforms during adult life: HbA and HbD (22). HbA is typically the major isoform, constituting ∼60–80% of adult Hb in passerine birds (22, 23). The major HbA isoform incorporates α-chain products of the α^A-globin gene, and the minor HbD isoform incorporates products of the α^D-globin gene; both isoforms incorporate β-chain products of the same β^A-globin gene. To characterize the red cell Hb isoform composition of house wrens, we analyzed blood samples from individual specimens using a combination of isoelectric focusing (IEF) and tandem mass spectrometry (MS/MS). Consistent with data from other passerines, our wild-caught house wrens expressed two distinct isoforms, HbA (pI = 8.7) and HbD (pI = 7.1–7.2). There was no clear difference in relative isoform abundance in house wrens from different elevations: the relative percentages of HbD were 39% and 42% in high- and low-altitude specimens, respectively [n = 14 (7 from >3,900 m and 7 from <395 m)]. MS/MS analysis confirmed that subunits of the two adult Hb isoforms represent products of the α^A-, α^D-, and β^A-globin genes; products of the embryonic α- and β-type globin genes were not detected.

Altitudinal Patterns of Amino Acid Polymorphism. In birds, as in other amniotes, the subfamilies of α- and β-type globin genes are located on different chromosomes (23–26). All oscine passerines examined to date possess three tandemly linked α-type globin genes and four tandemly linked β-type globin genes (22–24, 27). Because the proteomic analyses confirmed that subunits of the two adult-expressed Hb isoforms are exclusively encoded by the α^A-, α^D-, and β^A-globin genes, we surveyed nucleotide polymorphism at each of these three genes in the full panel of high- and low-altitude house wrens (n = 140) to identify amino acid changes that could potentially contribute to intraspecific variation in Hb function.

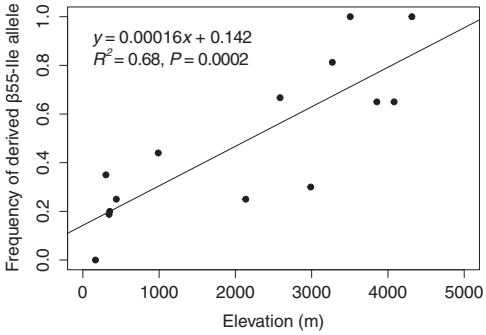

Fig. 1. The β55(Val/Ile) polymorphism exhibits a striking altitudinal pattern of allele frequency variation among 14 natural populations of house wrens from throughout Peru. The derived β55Ile allele predominates at high altitude and the ancestral Val allele predominates at lower altitudes.

This survey revealed a number of low-frequency amino acid polymorphisms, but only one polymorphism, β55(Val/Ile), exhibited a significantly nonrandom pattern of allele frequency variation with respect to altitude (Fig. 1 and Fig. S2). In the central Peru sample, the frequency of the derived Ile variant was 0.72 at high altitude and 0.31 at low altitude. This allele frequency difference of 0.41 was roughly twofold higher than that of any other amino acid polymorphism in the α- or β-globin genes. The three adult-expressed globin genes exhibited silent-site diversities of π = 0.0016–0.0105 in the total sample of Andean house wrens (Table S2).

Recurrent Substitutions at a Mutational Hot Spot. We sequenced the β^A-globin gene in 38 songbird species, including 15 species in the wren family (Troglodytidae) and 23 species representing nine families of oscine passerines. Phylogenetic analysis revealed that repeated nonsynonymous substitutions at the first codon position of β55 were attributable to the recurrent elimination of an ancestral CpG dinucleotide. Specifically, recurrent G→A transition substitutions at the first codon position converted β55Val to Ile in Andean house wrens and seven other passerine lineages, G→C transversion substitutions converted β55Val to Leu in several lineages, and successive A↔C transversions (non-CpG changes) interconverted β55Ile and Leu in thrushes (Fig. 2). Depending on the methylation status of the cytosine, eliminations of CpG dinucleotides via point mutations at either site are expected to occur at a far higher rate than non-CpG mutations at the same sites (16, 17). Consistent with this expectation, the estimated per-path rate for observed substitutions that eliminate the CpG dinucleotide (CpG→CpA and CpG→CpC) was approximately fivefold higher than the rate for other possible substitutions at the same site (0.0196 vs. 0.0043, respectively), and a likelihood ratio test indicated that the two-rate model provided a significantly better fit to the data than a single-rate model ($2\Delta\ln L$ = 4.75, P = 0.029).

Globin Gene Variation in Genome-Wide Context. For the purpose of making comparisons with patterns of variation in the adult-expressed α- and β-type globin genes of Andean house wrens, we surveyed intronic sequence polymorphism in the ρ- and β^H-globin genes, both of which are located immediately upstream of β^A-globin, and we also surveyed intronic sequence of the unlinked

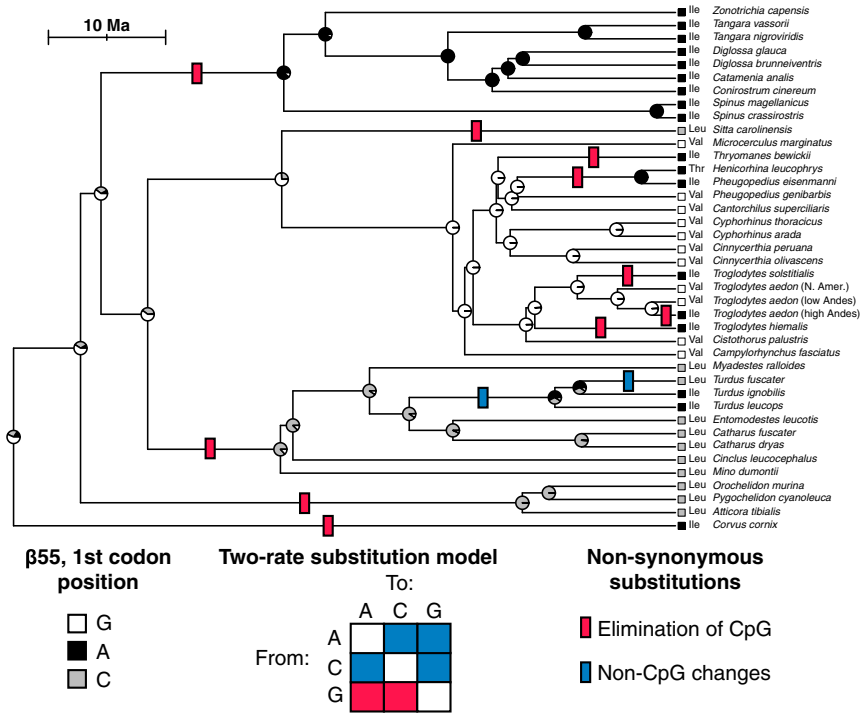

Fig. 2. Phylogeny of the wren family Troglodytidae and representative species from related oscine passerine families showing recurrent nonsynonymous substitutions at the first position of codon 55 in the β^A-globin gene. Blue and red tick marks indicate the minimum number of changes that are consistent with maximum-likelihood estimates of ancestral states at each node (see pie diagrams). An ancestral CpG dinucleotide was eliminated multiple times independently by nonsynonymous G→A transition substitutions (which produced β55Val→Ile replacements in Andean house wrens and several other passerine lineages) and G→C transversion substitutions (which produced β55Val→Leu replacements in multiple lineages). The third position of the codon immediately preceding β55 was cystosine (C) in all examined species except for *Cinclus leucocephalus*, which had thymine (T) and is part of a clade in which the CpG dinucleotide had already been eliminated by a CpG→CpC substitution. Depending on the methylation status of the cytosine, the rate of elimination of the CpG dinucleotide by point mutations at either site is expected to be ~10- to 15-fold higher than the mean mutation rate for non-CpG nucleotide sites. Maximum-likelihood analyses confirmed the expectation that the rate of substitutions that eliminated the CpG dinucleotide (CpG→CpA and CpG→CpC) was significantly higher than the rate of non-CpG substitutions at the same site.

myoglobin (Mb) gene. In comparisons between the high- and low-altitude population samples, the β^A-globin gene exhibited a higher level of nucleotide differentiation than each of the other linked and unlinked globin genes (Table S3).

To complement the multilocus survey of globin variation in the full panel of high- and low-altitude specimens, we used a subset of 28 specimens (14 highland, 14 lowland) in a genome-wide survey of single nucleotide polymorphisms (SNPs) in coding sequence. This allowed us to interpret altitudinal patterns of β55 polymorphism in a genome-wide context. We restricted the genomic analysis to 1,272 SNPs that mapped to putative protein-coding genes in a reference transcriptome (*SI Methods*). In the subset of specimens used in the genomic analysis, the site-specific F_{ST} value for β55 was 0.150, representing the upper 0.084 percentile of the empirical genome-wide distribution for coding SNPs. In the comparison between high- and low-altitude specimens comprising the central Peru sample (n = 108 alleles), the site-specific F_{ST} value for β55 was 0.269, representing the upper 0.013 percentile. The elevational differentiation in allele frequencies at the β55(Val/Ile) polymorphism thus provides suggestive evidence for a history of spatially varying selection.

Oxygenation Properties of Native HbA and HbD Variants. We purified HbA and HbD variants from highland and lowland house wren specimens that had representative globin genotypes. Measured differences in functional properties between the native HbA and HbD variants of highland and lowland house wrens reflect the net effects of naturally occurring allelic variation at two β-chain sites: β55(Val/Ile) and β80(Gly/Ser). Allelic variation at β80 contributes to amino acid heterogeneity in the set of specimens used in our functional experiments, but—unlike the β55(Val/Ile) polymorphism—it represents a low-frequency polymorphism in the global population and it does not exhibit a consistent altitudinal pattern of allele frequency variation (Fig. S3).

We measured O_2 equilibria of purified native Hb solutions under a standardized set of experimental treatments that enabled us to test for physiological differences in O_2 affinity between high- and low-altitude Hb variants while simultaneously providing insights into the molecular mechanism responsible for observed functional differences. We measured O_2 equilibria (*i*) in the absence of allosteric effectors ("stripped"), (*ii*) in the presence of Cl^- ions, added as 0.1 M KCl, (*iii*) in the presence of inositol hexaphosphate (IHP) (a chemical analog of the naturally occurring inositol pentaphosphate), at twofold molar excess over tetrameric Hb, and (*iv*) in the simultaneous presence of Cl^- and IHP. This latter treatment is most relevant to in vivo conditions in avian red blood cells. For each treatment, we estimated P_{50}, the PO_2 at which Hb is 50% saturated, and the Hill coefficient, n_{50}, a measure of cooperativity.

Because HbA and HbD share the same β-type subunit, functional effects of β-chain mutations should be manifest in comparisons between high- and low-altitude variants of both isoforms. Thus, data from both HbA and HbD provide replicate measurements of the mutations at β55 and β80 on two different α-chain backgrounds. The O_2 equilibrium measurements revealed pronounced differences in O_2 affinity between high- and low-altitude variants of both HbA and HbD (Table S4 and Fig. 3). $P_{50(KCl+IHP)}$ for the high-altitude HbA variant was 34% lower (O_2 affinity was higher) than that of the low-altitude variant (17.07 vs. 25.88 torr). Similarly, $P_{50(KCl+IHP)}$ for the high-altitude HbD variant was 17% lower than that of the low-altitude variant (13.45 vs. 16.29 torr). In high- and low-altitude samples, O_2 affinity differences between the two isoforms were consistent, as $P_{50(KCl+IHP)}$ was considerably higher for HbA relative to HbD (Table S4). Both isoforms exhibited cooperative O_2 binding, as estimated Hill coefficients (n_{50} values) in the KCl-plus-IHP treatment were 1.36–2.11 for HbA, and 2.28–2.36 for HbD (Table S4).

In the case of the high- and low-altitude HbA variants, the slight difference in intrinsic O_2 affinity [$P_{50(stripped)}$ = 2.47 vs. 2.80 torr, respectively] was greatly augmented in the presence of IHP and in the simultaneous presence of Cl^- and IHP (Table S4 and Fig. 3*A*). In the case of the HbD isoforms, there was no discernible difference in intrinsic O_2 affinity between the high- and low-altitude variants [$P_{50(stripped)}$ = 1.59 vs. 1.58 torr, respectively], but—as with the HbA variants—there was a highly significant affinity difference in the presence of Cl^- and IHP (Table S4 and Fig. 3*B*). Results for high- and low-altitude variants of HbA and HbD indicate that allelic differences in Hb function stem from changes in both intrinsic O_2 affinity and anion sensitivity. In both isoforms, these changes are clearly attributable to the independent or joint effect of shared amino acid mutations at β55 and β80.

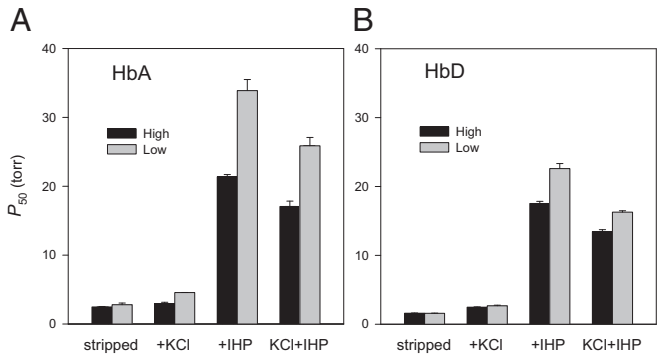

Fig. 3. O_2 affinities of HbA and HbD isoforms from high- and low-altitude populations of house wrens. (*A*) P_{50} values (mean ± SEM) for purified HbA variants of highland and lowland house wrens measured in 0.1 M Hepes buffer at pH 7.4 and 37 °C in the absence (stripped) and presence of allosteric effectors ([Cl^-], 0.1 M; IHP/Hb tetramer ratio, 2.0; [heme], 0.3 mM). (*B*) P_{50} values for HbD variants of highland and lowland wrens (experimental conditions as in *A*).

Functional Effects of Individual Mutations. To measure the relative contributions of the mutations β55Val→Ile and β80Gly→Ser, we used site-directed mutagenesis to engineer four recombinant Hb (rHb) mutants representing each possible genotypic combination of allelic variation at the two sites. The measured O_2 affinities of the ancestral genotype (55Val-80Ser) and the β55 single-mutant (55Ile-80Ser) recapitulated the measured difference between the native HbA variants from high- and low-altitude populations (Tables S4 and S5). The β55Val→Ile mutation produced a 25% reduction in $P_{50(KCl+IHP)}$ (an increase in O_2 affinity) on the ancestral 55Val-80Ser background (difference in P_{50} = 5.79 torr, 95% confidence limits of ΔP_{50} = 11.06, 0.52), and a 9% reduction on the background with the derived Gly at β80 (Fig. 4 and Table S5) (difference in P_{50} = 1.65 torr, 95% confidence limits of ΔP_{50} = 5.22, −1.92). The β80Ser→Gly mutation also had a substantial affinity-enhancing effect on the ancestral background (Fig. 4 and Table S5).

The Structural Mechanism Responsible for Changes in Hemoglobin–O_2 Affinity. Results of homology modeling suggest that the β55Val→Ile mutation increases intrinsic Hb–O_2 affinity through indirect effects on the β-chain distal heme pocket (the site of heme–ligand binding). The β55Val→Ile mutation results in the insertion of an additional carbonyl group in the $\alpha_1\beta_1$ intradimer gap between β55 and α119Pro, thereby forming a van der Waals contact between the two residues (Fig. 5). In the deoxy state, this added atomic contact at the $\alpha_1\beta_1$ interface induces strain on the adjacent D helix of the β-subunit, as indicated by a 1.3-fold increase in the single-residue frustration index for the derived β55Ile relative to Val on the ancestral background (Table S6). This effect propagates to the adjacent E helix, resulting in a subtle repositioning of key residues at the solvent interface that function as a gate for ligand entry/exit in the distal heme pocket and that directly or indirectly stabilize the heme–ligand complex (28).

Discussion

Possible Adaptive Significance of Altitudinal Differences in Hb–O_2 Affinity. The evolved difference in Hb–O_2 affinity between the highland and lowland house wrens is consistent with theoretical and empirical results demonstrating that the optimal blood–O_2 affinity varies according to the ambient PO_2, reflecting an unavoidable trade-off between the need to preserve arterial O_2 saturation under hypoxia while simultaneously ensuring adequate O_2 unloading in the peripheral circulation (29–31).

Patterns of convergence in Hb function among different high-altitude vertebrates also provide insights into the possible adaptive significance of changes in Hb–O_2 affinity. Comparative studies of Andean hummingbirds revealed that species with extraordinarily high elevational range limits consistently have higher Hb–O_2 affinities than closely related lowland species (32). Studies of birds and mammals have documented altitude-related differences in Hb–O_2 affinity in some cases (32–38), but not in others (39–42). Andean house wrens provide the first example (to our knowledge) of a continuously distributed bird species in which high-altitude natives have evolved a derived increase in Hb–O_2 affinity relative to lowland conspecifics. In contrast to recently documented cases where changes in Hb function between populations or closely related species evolved via multiple mutational changes that had individually minor effects (37, 38, 41), the increased Hb–O_2 affinity in high-altitude house wrens is clearly attributable to a single, large-effect mutation.

Insights into Structural Mechanism. Results of the protein-engineering experiments clearly demonstrate the affinity-enhancing effect of the β55Val→Ile mutation. A different amino acid substitution at this same site (β55Leu→Ser) has been implicated in the evolution of an increased Hb–O_2 affinity in the Andean goose (33, 34), although phylogenetic surveys of β^A-globin sequence variation have revealed that the β55Ser character state is not uniquely derived in the Andean goose—it is actually a shared, ancestral character state in South American sheldgeese, and most species in this group are lowland natives (43). The β55Leu→Ser substitution eliminates a van der Waals interaction between β55Leu and α119Pro at the $\alpha_1\beta_1$ intradimer interface, thereby destabilizing the T-state conformation and shifting the allosteric equilibrium in favor of the high-affinity R state, resulting in an increase in overall O_2 affinity. Engineering the same β55Leu→Ser substitution into recombinant human Hb produced the predicted increase in O_2 affinity, corroborating the hypothesized structural mechanism (33, 34).

In house wren Hb, an amino acid replacement at the same site also produces a dramatic change in O_2 affinity, but the structural mechanism is completely different. The affinity-enhancing β55Leu→Ser replacement in Andean goose Hb eliminates an atomic contact between α119 and β55, thereby destabilizing the low-affinity T-state conformation. By contrast, the affinity-enhancing β55Val→Ile replacement in house wren Hb adds an intradimer atomic contact in the same $\alpha_1\beta_1$ interface (Fig. 5), which indirectly affects deoxy β-heme reactivity by reorienting the E helix. This illustrates how substitutions involving different pairs of amino acid residues at the same site can alter protein function via different structural and functional mechanisms.

Effects of Mutation Bias on Propensities of Molecular Adaptation. Results of our molecular evolution analysis demonstrated a quantitative asymmetry in rates of CpG and non-CpG substitution in the first codon position of β55, and results of our protein-engineering experiments demonstrated that the mutationally favored

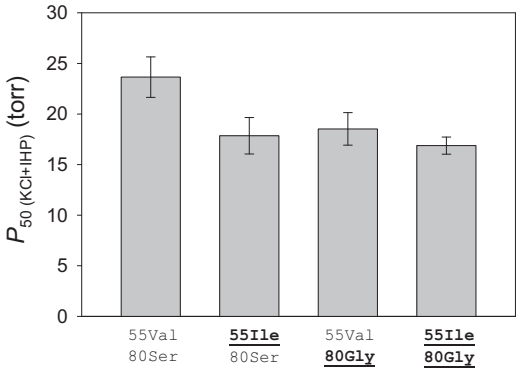

Fig. 4. O_2 affinities [$P_{50(KCl+IHP)}$, torr; mean ± SEM] of purified house wren rHb mutants measured in the presence of physiological concentrations of Cl^- ions (0.1 M KCl) and IHP (at twofold molar excess over tetrameric Hb). O_2 equilibrium curves for each rHb mutant were measured in 0.1 M Hepes buffer at pH 7.40, 37 °C, and [heme], 0.3 mM. Numbers refer to residue positions in the β-chain subunit. "55Ile-80Ser" and "55Val-80Ser" are the two-site genotypes that predominate in high- and low-altitude house wrens, respectively. At each site, the derived (nonancestral) amino acid residues are underlined.

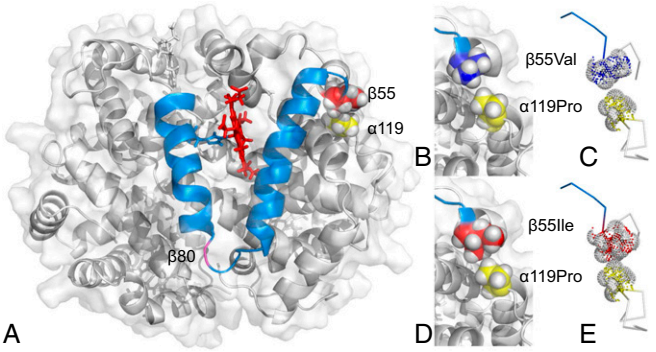

Fig. 5. Homology model of house wren HbA showing the location of amino acid replacements that distinguish high- and low-altitude variants. (*A*) The E and F helices of the β-chain subunit are shown in blue. The side chain of the proximal histidine, β92 (which covalently binds the fifth coordination site of the heme iron) is also shown in blue, and the residues forming the $\alpha_1\beta_1$ intradimer contact between β55 and α119 are shown in red and yellow, respectively, with space-filling representation of van der Waals radii. The site of the β80Ser→Gly mutation in the EF interhelical loop is shown in pink. (*B* and *C*) There is no interchain atomic contact between β55Val and α119Pro at the $\alpha_1\beta_1$ contact surface. (*D* and *E*) Because Ile has an additional carbon atom relative to Val, a van der Waals interaction is formed between β55Ile and α119Pro.

Val→Ile replacement at this site produces a significant increase in Hb–O_2 affinity on the ancestral genetic background (Fig. 4 and Table S5). The direction of character state change is consistent with the expectation that an increased Hb–O_2 affinity is adaptive at high altitude. This inference is bolstered by results of the population genomic analysis, which suggest that the altitudinal shift in frequency of the derived β55-Ile variant is attributable to a history of spatially varying selection. Our results therefore demonstrate how a mutationally favored amino acid change produced a large phenotypic effect that has likely adaptive significance. The important question is whether the increased rate of mutation to the function-altering allele made the observed evolutionary outcome especially likely to occur. This is relevant to the more general question of whether propensities of mutational change cause propensities in pathways of adaptive molecular evolution (10, 11, 44, 45).

Studies of naturally occurring mutations in human Hb and engineered mutations in recombinant Hbs, as well as comparative studies of Hbs from different animal species, demonstrate that there are numerous possible amino acid changes that are capable of producing fine-tuned increases in Hb–O_2 affinity (46–49). As an adaptive solution to the respiratory challenges of O_2 transport at high altitude, there is no reason to think that the β55Val→Ile replacement was a forced option; any number of amino acid mutations in the same protein presumably could have produced a quantitatively similar phenotypic effect. Assuming that an increased Hb–O_2 affinity confers a fitness benefit in birds living at high altitude, there seems little reason to suppose that the observed β55Val→Ile mutation would have had a higher fixation probability than any number of other possible affinity-enhancing mutations. However, if the rate of β55Val→Ile mutation is 10-fold higher than the rate of mutation to any other affinity-enhancing amino acid at any other site in the protein, then—in the absence of contributions from standing variation—this would bias evolutionary outcomes in the same way as a 10-fold higher probability of fixation. When adaptive evolution is mutation-limited, an increase in the rate of mutation to a particular allele and a commensurate increase in the mutant allele's probability of fixation have the same effect on the odds that the allele will be the next to fix (4, 10, 11, 50). The extent to which adaptation in natural populations approximates the mutation-limited scenario envisioned by origin-fixation models remains an open question in evolutionary genetics (50). Our findings suggest that variation in the mutation rate to function-altering alleles may be an important factor influencing the preferential fixation of mutations during phenotypic evolution.

Methods

Sample Collection. We collected 140 house wren specimens from a range of elevations (120–4,454 m above sea level) in the Peruvian Andes and adjacent lowlands. All specimens were preserved as vouchers in the ornithological collection of the Museum of Southwestern Biology of the University of New Mexico and the Centro de Ornitología y Biodiversidad (CORBIDI) (Lima, Peru). Birds were handled in accordance with protocols approved by the University of New Mexico Institutional Care and Use Committee (Protocol 08UNM033-TR-100117; Animal Welfare Assurance number A4023-01). Complete specimen data are available via the ARCTOS online database (Table S1). Details regarding specimen collection and permits are provided in *SI Methods*.

Characterization of Hb Isoform Composition. We characterized Hb isoform composition in the mature erythrocytes of 14 house wren specimens (7 highland and 7 lowland). Native Hb components were separated by means of IEF, gel bands were excised and digested with trypsin, and MS/MS was used to identify the resultant peptides, as described in *SI Methods*.

Molecular Cloning and Sequencing. Details regarding cloning and sequencing protocols are provided in *SI Methods*. All sequences were deposited in GenBank under accession numbers KT759682–KT760400.

Phylogenetic Survey of β^A-Globin Sequence Variation in Oscine Passerines. We sequenced the β^A-globin gene in representative wren species and species from related oscine passerine families. We used a time-scaled supertree (51) and the "ace" function of the R package *ape* (52) to test alternative maximum-likelihood models of character state change and to estimate ancestral character states for the first codon position of β55. Our model was based on a 3 × 3 rate matrix representing all possible interconversions among observed character states at the focal site: A, C, and G (T was not an observed character state). The null model used a single rate parameter for all six substitution types. The alternative model included a second rate parameter for substitutions that eliminated the CpG dinucleotide (CpG→CpA and CpG→CpC). We used a likelihood ratio test to compare the one-rate and two-rate models.

Population Genetic Analysis. For each of the adult-expressed globin genes (α^A-, α^D-, and β^A-globin), we computed summary statistics of nucleotide polymorphism, as described in *SI Methods*.

Survey of Genomic Differentiation. We used a genotyping-by-sequencing approach to survey genome-wide patterns of nucleotide differentiation in coding sequence. Briefly, we used genomic DNA samples from 28 house wren specimens to produce multiplexed, reduced-representation Illumina libraries. Details of library preparation, library sequencing, and quality control filtering are provided in *SI Methods*. Parsed Illumina reads have been deposited in the National Center for Biotechnology Information Sequence Read Archive (SRA) (PRJNA295865).

Protein Purification and in Vitro Analysis of Hb Function. The experimental analysis of native HbA and HbD variants was based on pooled hemolysates from seven highland specimens and seven lowland specimens that had representative genotypes. For each of the pooled hemolysates, we isolated and purified the HbA and HbD isoforms by means of anion-exchange fast-protein liquid chromatography, using a HiTrap QHP column (GE Healthcare). Details regarding sample preparation and the measurement of O_2 equilibrium curves are provided in *SI Methods*.

Vector Construction and Site-Directed Mutagenesis. The α^A- and β^A-globin sequences were synthesized by Eurofins MWG Operon after optimizing the nucleotide sequences in accordance with *Escherichia coli* codon preferences. The synthesized α^A-β^A globin gene cassette was cloned into a custom pGM vector system along with the *methionine aminopeptidase* (MAP) gene, as described previously (37, 53). We engineered each of the β-chain codon substitutions using the QuikChange II XL Site-Directed Mutagenesis kit from Stratagene. Each engineered codon change was verified by DNA sequencing.

Expression and Purification of Recombinant Hbs. Recombinant Hb expression was carried out in the *E. coli* JM109 (DE3) strain as described previously (53). Additional details are provided in *SI Methods*.

Structural Modeling. Homology-based structural modeling was performed on the SWISS-MODEL server (54), using human deoxyHb (Protein Data Bank ID 2hhb) as template. To predict mutational effects on conformational stress, we computed an index of energetic frustration using the Frustratometer program (55). Graphics were produced by the PyMol (Schrödinger).

ACKNOWLEDGMENTS. We thank the Peruvian government agencies Instituto Nacional de Recursos Naturales and Servicio Nacional Forestal y de Fauna Silvestre for permits. We thank T. Valqui, E. Bautista, and CORBIDI for assistance in the field; J. Projecto-Garcia and E. Ellebæk Petersen for assistance in the laboratory; and two anonymous reviewers for constructive criticism. This work was funded by the Frank M. Chapman Fund of the American Museum of Natural History (S.C.G.); the Department of Animal Biology, University of Illinois (Z.A.C.); the National Institutes of Health/National Heart, Lung, and Blood Institute [Grant HL087216 (to J.F.S.)]; the National Science Foundation [Grant IOS-0949931 (to J.F.S.), Grant IOS-1354390 (to J.F.S.), Grant MCB-1517636 (to J.F.S.), Grant IOS-1354934 (to Z.A.C.), Grant DEB-1146491 (to C.C.W.), and Grant MCB-1516660 (to C.C.W.)]; the Danish Council for Independent Research, Natural Sciences [Grant 10-084-565 (to A.F.)]; and the Faculty of Science and Technology, Aarhus University (R.E.W.).

1. Stern DL, Orgogozo V (2008) The loci of evolution: How predictable is genetic evolution? *Evolution* 62(9):2155–2177.
2. Stern DL, Orgogozo V (2009) Is genetic evolution predictable? *Science* 323(5915):746–751.
3. Gompel N, Prud'homme B (2009) The causes of repeated genetic evolution. *Dev Biol* 332(1):36–47.
4. Streisfeld MA, Rausher MD (2011) Population genetics, pleiotropy, and the preferential fixation of mutations during adaptive evolution. *Evolution* 65(3):629–642.
5. Stern DL (2013) The genetic causes of convergent evolution. *Nat Rev Genet* 14(11):751–764.
6. Nei M (2013) *Mutation-Driven Evolution* (Oxford Univ Press, Oxford).
7. Otto SP (2004) Two steps forward, one step back: The pleiotropic effects of favoured alleles. *Proc Biol Sci* 271(1540):705–714.
8. Carroll SB (2008) Evo-devo and an expanding evolutionary synthesis: A genetic theory of morphological evolution. *Cell* 134(1):25–36.
9. Chevin L-M, Martin G, Lenormand T (2010) Fisher's model and the genomics of adaptation: Restricted pleiotropy, heterogenous mutation, and parallel evolution. *Evolution* 64(11):3213–3231.
10. Yampolsky LY, Stoltzfus A (2001) Bias in the introduction of variation as an orienting factor in evolution. *Evol Dev* 3(2):73–83.
11. Stoltzfus A (2006) Mutation-biased adaptation in a protein NK model. *Mol Biol Evol* 23(10):1852–1862.
12. Chan YF, et al. (2010) Adaptive evolution of pelvic reduction in sticklebacks by recurrent deletion of a *Pitx1* enhancer. *Science* 327(5963):302–305.
13. Nachman MW, Crowell SL (2000) Estimate of the mutation rate per nucleotide in humans. *Genetics* 156(1):297–304.
14. Kondrashov AS (2003) Direct estimates of human per nucleotide mutation rates at 20 loci causing Mendelian diseases. *Hum Mutat* 21(1):12–27.
15. Webster MT, Axelsson E, Ellegren H (2006) Strong regional biases in nucleotide substitution in the chicken genome. *Mol Biol Evol* 23(6):1203–1216.
16. Ellegren H (2013) The evolutionary genomics of birds. *Annu Rev Ecol Evol Syst* 44:239–259.
17. Fjeldsa J, Kessler M (1990) *Birds of the High Andes* (University of Copenhagen and Apollo Books, Svendborg, Denmark).
18. Storz JF, Scott GR, Cheviron ZA (2010) Phenotypic plasticity and genetic adaptation to high-altitude hypoxia in vertebrates. *J Exp Biol* 213(Pt 24):4125–4136.
19. Smith BT, Klicka J (2010) The profound influence of the Late Pliocene Panamanian uplift on the exchange, diversification, and distribution of New World birds. *Ecography* 33(2):333–342.
20. Galen SC, Witt CC (2014) Diverse avian malaria and other haemosporidian parasites in Andean house wrens: Evidence for regional co-diversification by host-switching. *J Avian Biol* 45(4):374–386.
21. Perutz MF (1989) Mechanisms of cooperativity and allosteric regulation in proteins. *Q Rev Biophys* 22(2):139–237.
22. Grispo MT, et al. (2012) Gene duplication and the evolution of hemoglobin isoform differentiation in birds. *J Biol Chem* 287(45):37647–37658.
23. Opazo JC, et al. (2015) Gene turnover in the avian globin gene families and evolutionary changes in hemoglobin isoform expression. *Mol Biol Evol* 32(4):871–887.
24. Hoffmann FG, Storz JF, Gorr TA, Opazo JC (2010) Lineage-specific patterns of functional diversification in the α- and β-globin gene families of tetrapod vertebrates. *Mol Biol Evol* 27(5):1126–1138.
25. Hoffmann FG, Opazo JC, Storz JF (2012) Whole-genome duplications spurred the functional diversification of the globin gene superfamily in vertebrates. *Mol Biol Evol* 29(1):303–312.
26. Storz JF, Opazo JC, Hoffmann FG (2013) Gene duplication, genome duplication, and the functional diversification of vertebrate globins. *Mol Phylogenet Evol* 66(2):469–478.
27. Zhang G, et al.; Avian Genome Consortium (2014) Comparative genomics reveals insights into avian genome evolution and adaptation. *Science* 346(6215):1311–1320.
28. Birukou I, Soman J, Olson JS (2011) Blocking the gate to ligand entry in human hemoglobin. *J Biol Chem* 286(12):10515–10529.
29. Turek Z, Kreuzer F, Turek-Maischeider M, Ringnalda BEM (1978) Blood O_2 content, cardiac output, and flow to organs at several levels of oxygenation in rats with a left-shifted blood oxygen dissociation curve. *Pflugers Arch* 376(3):201–207.
30. Bencowitz HZ, Wagner PD, West JB (1982) Effect of change in P_{50} on exercise tolerance at high altitude: A theoretical study. *J Appl Physiol* 53(6):1487–1495.
31. Willford DC, Hill EP, Moores WY (1982) Theoretical analysis of optimal P_{50}. *J Appl Physiol* 52(4):1043–1048.
32. Projecto-Garcia J, et al. (2013) Repeated elevational transitions in hemoglobin function during the evolution of Andean hummingbirds. *Proc Natl Acad Sci USA* 110(51):20669–20674.
33. Jessen TH, Weber RE, Fermi G, Tame J, Braunitzer G (1991) Adaptation of bird hemoglobins to high altitudes: Demonstration of molecular mechanism by protein engineering. *Proc Natl Acad Sci USA* 88(15):6519–6522.
34. Weber RE, Jessen TH, Malte H, Tame J (1993) Mutant hemoglobins (α 119-Ala and β 55-Ser): Functions related to high-altitude respiration in geese. *J Appl Physiol (1985)* 75(6):2646–2655.
35. Storz JF, et al. (2009) Evolutionary and functional insights into the mechanism underlying high-altitude adaptation of deer mouse hemoglobin. *Proc Natl Acad Sci USA* 106(34):14450–14455.
36. Storz JF, Runck AM, Moriyama H, Weber RE, Fago A (2010) Genetic differences in hemoglobin function between highland and lowland deer mice. *J Exp Biol* 213(Pt 15):2565–2574.
37. Natarajan C, et al. (2013) Epistasis among adaptive mutations in deer mouse hemoglobin. *Science* 340(6138):1324–1327.
38. Tufts DM, et al. (2015) Epistasis constrains mutational pathways of hemoglobin adaptation in high-altitude pikas. *Mol Biol Evol* 32(2):287–298.
39. Revsbech IG, et al. (2013) Hemoglobin function and allosteric regulation in semi-fossorial rodents (family Sciuridae) with different altitudinal ranges. *J Exp Biol* 216(Pt 22):4264–4271.
40. Cheviron ZA, et al. (2014) Integrating evolutionary and functional tests of adaptive hypotheses: A case study of altitudinal differentiation in hemoglobin function in an Andean sparrow, *Zonotrichia capensis*. *Mol Biol Evol* 31(11):2948–2962.
41. Natarajan C, et al. (2015) Intraspecific polymorphism, interspecific divergence, and the origins of function-altering mutations in deer mouse hemoglobin. *Mol Biol Evol* 32(4):978–997.
42. Janecka JE, et al. (2015) Genetically based low oxygen affinities of felid hemoglobins: Lack of biochemical adaptation to high-altitude hypoxia in the snow leopard. *J Exp Biol* 218(Pt 15):2402–2409.
43. McCracken KG, Barger CP, Sorenson MD (2010) Phylogenetic and structural analysis of the HbA (alphaA/betaA) and HbD (alphaD/betaA) hemoglobin genes in two high-altitude waterfowl from the Himalayas and the Andes: Bar-headed goose (*Anser indicus*) and Andean goose (*Chloephaga melanoptera*). *Mol Phylogenet Evol* 56(2):649–658.
44. Stoltzfus A (2006) Mutationism and the dual causation of evolutionary change. *Evol Dev* 8(3):304–317.
45. Stoltzfus A, Yampolsky LY (2009) Climbing mount probable: Mutation as a cause of nonrandomness in evolution. *J Hered* 100(5):637–647.
46. Bellelli A, Brunori M, Miele AE, Panetta G, Vallone B (2006) The allosteric properties of hemoglobin: Insights from natural and site directed mutants. *Curr Protein Pept Sci* 7(1):17–45.
47. Weber RE (2007) High-altitude adaptations in vertebrate hemoglobins. *Respir Physiol Neurobiol* 158(2-3):132–142.
48. Storz JF, Moriyama H (2008) Mechanisms of hemoglobin adaptation to high altitude hypoxia. *High Alt Med Biol* 9(2):148–157.
49. Varnado CL, et al. (2013) Development of recombinant hemoglobin-based oxygen carriers. *Antioxid Redox Signal* 18(17):2314–2328.
50. McCandlish DM, Stoltzfus A (2014) Modeling evolution using the probability of fixation: History and implications. *Q Rev Biol* 89(3):225–252.
51. Jetz W, Thomas GH, Joy JB, Hartmann K, Mooers AO (2012) The global diversity of birds in space and time. *Nature* 491(7424):444–448.
52. Paradis E, Claude J, Strimmer K (2004) APE: Analyses of Phylogenetics and Evolution in R language. *Bioinformatics* 20(2):289–290.
53. Natarajan C, et al. (2011) Expression and purification of recombinant hemoglobin in *Escherichia coli*. *PLoS One* 6(5):e20176.
54. Biasini M, et al. (2014) SWISS-MODEL: Modelling protein tertiary and quaternary structure using evolutionary information. *Nucleic Acids Res* 42(Web Server issue):W252–W258.
55. Jenik M, et al. (2012) Protein frustratometer: A tool to localize energetic frustration in protein molecules. *Nucleic Acids Res* 40(Web Server issue):W348–W351.
56. Hoffmann FG, Storz JF (2007) The alphaD-globin gene originated via duplication of an embryonic α-like globin gene in the ancestor of tetrapod vertebrates. *Mol Biol Evol* 24(9):1982–1990.
57. Hudson RR (1987) Estimating the recombination parameter of a finite population model without selection. *Genet Res* 50(3):245–250.
58. Parchman TL, et al. (2012) Genome-wide association genetics of an adaptive trait in lodgepole pine. *Mol Ecol* 21(12):2991–3005.
59. Balakrishnan CN, et al. (2014) Brain transcriptome sequencing and assembly of three songbird model systems for the study of social behavior. *PeerJ* 2:e396.
60. Langmead B, Salzberg SL (2012) Fast gapped-read alignment with Bowtie 2. *Nat Methods* 9(4):357–359.
61. Catchen J, Hohenlohe PA, Bassham S, Amores A, Cresko WA (2013) Stacks: An analysis tool set for population genomics. *Mol Ecol* 22(11):3124–3140.
62. Weber RE (1992) Use of ionic and zwitterionic (Tris/BisTris and HEPES) buffers in studies on hemoglobin function. *J Appl Physiol (1985)* 72(4):1611–1615.
63. Storz JF, Weber RE, Fago A (2012) Oxygenation properties and oxidation rates of mouse hemoglobins that differ in reactive cysteine content. *Comp Biochem Physiol A Mol Integr Physiol* 161(2):265–270.
64. Weber RE, Fago A, Malte H, Storz JF, Gorr TA (2013) Lack of conventional oxygen-linked proton and anion binding sites does not impair allosteric regulation of oxygen binding in dwarf caiman hemoglobin. *Am J Physiol Regul Integr Comp Physiol* 305(3):R300–R312.

Supporting Information

Galen et al. 10.1073/pnas.1507300112

SI Methods

Sample Collection. All birds were live-trapped in mist nets and were sacrificed in accordance with protocols approved by the University of New Mexico Institutional Care and Use Committee (Protocol 08UNM033-TR-100117; Animal Welfare Assurance number A4023-01). All collections were authorized by permits issued by management authorities of Peru (004-2007-INRENA-IFFS-DCB, 135-2009-AG-DGFFS-DGEFFS, 0377-2010-AG-DGFFS-DGEFFS, 0199-2012-AG-DGFFS-DGEFFS, and 006-2013-MINAGRI-DGFFS/DGEFFS).

For each of the 140 house wren specimens, we collected 20–60 μL of whole blood from the brachial or ulnar vein using heparinized microcapillary tubes. Red blood cells were separated from the plasma fraction by centrifugation, and the packed red cells were flash-frozen in liquid nitrogen. We collected liver and pectoral muscle from each specimen as sources of genomic DNA and globin mRNA, respectively. Muscle samples were flash-frozen or preserved using RNAlater. All tissue and blood samples were subsequently stored at −80 °C.

Tandem Mass Spectrometry. Database searches of MS/MS spectra were performed using Mascot (Matrix Science; version 1.9.0). Specifically, peptide mass fingerprints derived from the MS/MS analysis were used to query a custom database of avian α- and β-type globin sequences. These amino acid sequences were derived from conceptual translations of the adult-expressed α^A-, α^D-, and β^A-globin genes of *T. aedon*, in addition to the full complement of embryonic and adult α- and β-type globin genes that have been annotated in the genome assemblies of other birds (22–24, 27, 56). We identified all significant protein hits that matched more than one peptide with $P < 0.05$. After separating the HbA and HbD isoforms by native gel IEF and identifying each band on the gel by MS/MS, the relative abundance of the different isoforms was quantified densitometrically.

PCR, Cloning, and Sanger Sequencing. We extracted genomic DNA from frozen tissues of each of the 140 house wren specimens using the DNeasy Blood and Tissue Kit (Qiagen). We used the PCR to amplify six autosomal loci, including full-length coding sequences of the adult-expressed α- and β-type globin genes (α^A-, α^D-, and β^A-globin), intron 2 sequences of ρ-globin and β^H-globin (β-type globin genes that are located just upstream of β^A-globin), and intron 2 of the unlinked myoglobin gene. Negative controls were included in each PCR to control for contamination. All PCR amplicons were purified using ExoSap-IT (USB) and were sequenced in both directions using dye terminator cycle-sequencing (BigDye; ABI) on an ABI 3130 automated sequencer (Applied Biosystems).

For the 14 specimens used in the experimental analyses of Hb function, we extracted RNA from pectoral muscle tissue using the RNeasy kit (Qiagen) and we amplified full-length cDNAs of the α^A, α^D-, and β^A-globin genes using a OneStep RT-PCR kit (Qiagen). We designed paralog-specific primers using 5′- and 3′-UTR sequences from passerine species, as described previously (23). We cloned RT-PCR products using the TOPO TA Cloning Kit (Life Technologies), and we sequenced at least five clones per gene to recover both alleles of each globin gene. This enabled us to determine full diploid genotypes for each of the three adult-expressed globin genes in each specimen.

Population Genetic Analysis. We computed summary statistics of nucleotide polymorphism for each of the adult-expressed globin genes (α^A-, α^D-, and β^A-globin). As a measure of nucleotide variation, we calculated nucleotide diversity, π, and Watterson's θ_W, an estimator of the population mutation rate (=$4N\mu$, where N is the effective population size and μ is the mutation rate per nucleotide). We calculated Tajima's D to characterize the distribution of allele frequencies at silent sites and we calculated Hudson's (57) estimator of the population recombination rate, $4Nc$, where c is the rate of crossing over between adjacent nucleotides. To test whether measured values of Tajima's D deviated from neutral-equilibrium expectations, we obtained critical values for each statistic by conducting 10,000 coalescent simulations (no recombination) that were conditioned on the observed number of segregating sites.

Genome-Wide Survey of Nucleotide Differentiation Using a Genotyping-by-Sequencing Approach. To more broadly survey patterns of genomic differentiation between high- and low-elevation populations, we produced multiplexed, reduced-representation Illumina libraries following Parchman et al. (58). Briefly, we digested genomic DNA samples for a total of 28 individuals (14 from high elevation and 14 from low elevation; Table S1) with two restriction endonucleases (EcoRI and Mse1). We then ligated double-stranded adaptor oligonucleotides that contained Illumina sequencing binding sites and a unique 8- to 10-bp barcode for individual identification, and PCR amplified these adaptor-ligated fragments. Details on the adaptor sequences as well as the digestion and PCR conditions can be found in the study by Parchman et al. (58). We pooled the barcoded amplicons from each individual in equimolar concentrations, and electrophoresed them on 2.5% agarose gel for size selection. Fragments that were between 350 and 500 bp in length were excised from the gel and purified using a QIAquick Gel Extraction Kit (Qiagen). The pooled library was sequenced in a single lane on the Illumina HiSEq 1000 platform as 100-nt single-end reads at the Keck Center for Comparative and Functional Genomics at the University of Illinois, Urbana–Champaign.

We parsed the resulting reads by individual barcodes and trimmed adaptor sequences and low-quality bases using custom Perl scripts, resulting in a final mean read length of 87 nt. To limit our analysis to putative protein-coding genes, we mapped individual *T. aedon* reads to the published transcriptome of a closely related passerine, *Zontrichia leucophrys* (59), using the *sensitive-local* settings in Bowtie2 (60). Transcript-aligned reads were then processed using the program STACKS (61) to identify single-nucleotide polymorphisms (SNPs) in reads that mapped to known transcripts using the following input parameters for pstacks: - m3, –model_type snp, –alpha 0.05. All 28 individuals were included when compiling the SNP catalog in cstacks. Downstream population genetic analysis were restricted to loci that were genotyped in at least 10 individuals per population with a minimum sequencing depth of 5 reads per locus per individual and a minor allele frequency of 0.05, resulting in a final dataset of 1,272 unique loci. We calculated locus-specific F_{ST} values using the program POPULATIONS implemented in STACKS (61).

Protein Purification and in Vitro Analysis of Hb Function. We purified HbA and HbD variants from pooled hemolysates from seven highland specimens and seven lowland specimens. There was a nearly fixed difference between the two samples at β55, with Ile and Val alleles predominating in the highland and lowland specimens, respectively, but there was also a low level of amino acid heterogeneity at site β80: a derived Gly allele was present at

frequencies of 0.36 and 0.07 in the samples of highland and lowland specimens, respectively (n = 14 alleles in each sample).

Using purified Hb solutions (0.3 mM heme) that were stripped of organic phosphates and other allosteric effectors, we measured O_2 equilibrium curves at 37 °C, 0.1 M Hepes, pH 7.4, in the absence ("stripped") and presence of 0.1 M KCl, IHP (at twofold molar excess over tetrameric Hb), and in the simultaneous presence of KCl and IHP. We measured O_2 equilibria of 3-μL thin-film samples in a modified diffusion chamber where absorption at 436 nm was monitored during stepwise changes in equilibration gas mixtures generated by precision Wösthoff gas-mixing pumps. We estimated values of P_{50} and n_{50} (Hill's cooperativity coefficient at half-saturation) by fitting the Hill equation $Y = PO_2^n/(P_{50}^n + PO_2^n)$ to the experimental O_2 saturation data by means of nonlinear regression (Y = fractional O_2 saturation; n, cooperativity coefficient) (22, 62–64). The model fitting was based on five to eight equilibration steps between 30% and 70% oxygenation. Free Cl^- concentrations were measured with a model 926S Mark II chloride analyzer (Sherwood Scientific Ltd.).

Expression and Purification of Recombinant Hbs. Recombinant Hb expression was carried out in the JM109 (DE3) *E. coli* strain. Bacterial cells were selected in LB agar with dual antibiotics (ampicillin and kanamycin) to ensure that transformants received both pGM and pCO-MAP plasmids for expression. The expression of each rHb mutant was carried out in 1.5 L of TB medium. Bacterial cells were grown in 37 °C in an orbital shaker at 200 rpm until absorbance values reached 0.6–0.8 at 600 nm. The bacterial cultures were induced by 0.2 mM isopropyl β-D-1-thiogalactopyranoside and were then supplemented with hemin (50 μg/mL) and glucose (20 g/L). The bacterial culture conditions and the protocol for preparing cell lysates are described in the study by Natarajan et al. (53).

We purified each rHb sample by means of two step ion-exchange chromatography as described previously (32, 37, 38, 40, 53). Samples were passed through a cation-exchange column (HiTrap SP-Sepharose; GE Healthcare; 17-1152-01) followed by equilibration with 20 mM Tris buffer (0.5 mM EDTA, 0.5 mM DTT, pH 6.0) and elution using a linear gradient of 0–0.5 M NaCl. The eluted fractions were passed through an anion-exchange column (HiTrap Q-Sepharose; GE Healthcare; 17-1153-01), followed by equilibration with 20 mM Tris buffer (0.5 mM EDTA, 0.5 mM DTT, pH 8.5), and elution using a linear gradient of 0–0.5 M NaCl. The samples were desalted by dialysis against 10 mM Hepes buffer (pH 7.6) at 4 °C. The eluted fractions of each rHb sample were concentrated by using centrifugal filtrate. The purified rHb samples were analyzed by SDS-polyacrylamide gel electrophoresis and isoelectrofocusing (IEF). After preparing rHb samples as oxyHb, deoxyHb, and carbonmonoxy derivatives, we measured absorbance at 450–600 nm to confirm that the absorbance maxima match those of the native HbA samples.

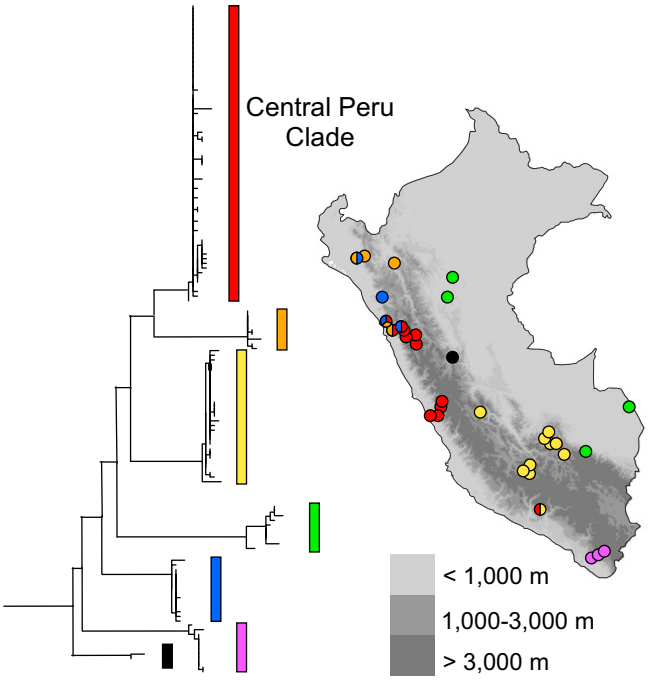

Fig. S1. Phylogeographic population structure of house wrens sampled from throughout Peru. The tree (*Left*) shows relationships among well-defined mtDNA clades. In the map (*Right*), color coding of symbols shows the proportional representation of different mtDNA clades in samples of house wren specimens from each locality. Specimens comprising the "central Peru clade" served as the focus for the elevational survey of genomic polymorphism, as described in the main text.

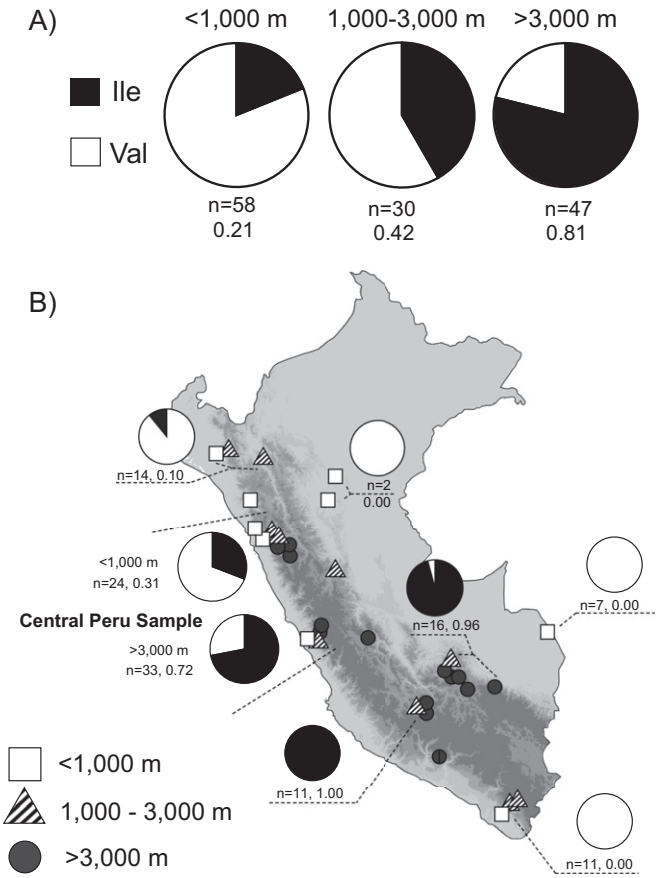

Fig. S2. The β55(Val/Ile) polymorphism exhibits a striking altitudinal pattern of allele frequency variation in natural populations of Peruvian house wrens. (*A*) The β55Ile allele predominates at high altitude, and the Val allele predominates at lower altitudes. (*B*) Variation in frequency of the derived β55Ile allele across Peru. The central Peru sample comprises a phylogeographically defined set of specimens that served as the focus for the elevational survey of genomic polymorphism.

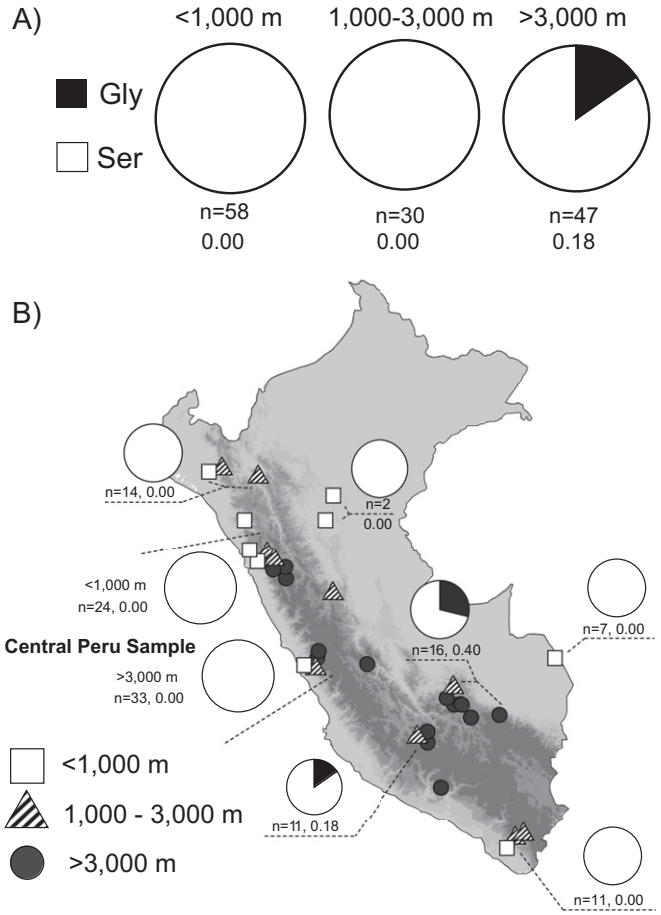

Fig. S3. In addition to the β55(Val/Ile) polymorphism, β80 is one of the only other amino acid sites that harbors segregating variation in natural populations of Peruvian house wrens. However, the ancestral Ser allele predominates in population samples from every elevational zone. (*A*) The derived β80Gly allele is present at moderate frequencies in population samples from the highlands of southern Peru. (*B*) Variation in frequency of the derived β80Gly allele across Peru. The central Peru sample comprises a phylogeographically defined set of specimens that served as the focus for the elevational survey of genomic polymorphism.

Table S1. House wren samples used in this study with ARCTOS Museum of Southwestern Biology catalog web link, sampling details, and mtDNA clade from Galen and Witt (20)

Catalog no. with embedded web link	NK	Day	Month	Elevation, m	Department	Latitude	Longitude	mtDNA clade
MSB:Bird:27052	159705	30	Oct	3,040	Lima	−11.76	−76.58	1
MSB:Bird:27596	162008	3	Jun	366	Lima	−12.01	−76.92	1
MSB:Bird:27606	162022	3	Jun	366	Lima	−12.01	−76.92	1
MSB:Bird:27609	162025	3	Jun	366	Lima	−12.01	−76.92	1
MSB:Bird:31418	162982	8	Jan	372	Lima	−12	−76.92	1
MSB:Bird:31425	162989	8	Jan	351	Lima	−12	−76.92	1
MSB:Bird:31433	162997	8	Jan	372	Lima	−12	−76.92	1
MSB:Bird:31450	163014	9	Jan	352	Lima	−12.01	−76.92	1
MSB:Bird:31454	163018	9	Jan	352	Lima	−12.01	−76.92	1
MSB:Bird:31456	163020	9	Jan	352	Lima	−12.01	−76.92	1
MSB:Bird:31459	163023	9	Jan	352	Lima	−12.01	−76.92	1
MSB:Bird:31469	163033	12	Jan	3,967	Lima	−11.63	−76.43	1
MSB:Bird:31482	163046	12	Jan	3,959	Lima	−11.63	−76.43	1
MSB:Bird:31489	163053	13	Jan	3,973	Lima	−11.63	−76.43	1
MSB:Bird:31498	163062	13	Jan	3,981	Lima	−11.63	−76.43	1
MSB:Bird:31503	163067	14	Jan	3,967	Lima	−11.63	−76.43	1
MSB:Bird:31739	163411	7	May	3,750	Lima	−11.76	−76.55	1
MSB:Bird:31756	163428	21	May	2,400	Lima	−11.74	−76.61	1
MSB:Bird:31766	163438	24	May	2,400	Lima	−11.74	−76.61	1
MSB:Bird:31767	163439	24	May	2,400	Lima	−11.74	−76.61	1
MSB:Bird:32902	168074	15	Oct	935	Lima	−12.03	−76.65	1
MSB:Bird:32909	168081	15	Oct	935	Lima	−12.03	−76.65	1
MSB:Bird:32910	168082	15	Oct	935	Lima	−12.03	−76.65	1
MSB:Bird:32922	168094	16	Oct	935	Lima	−12.03	−76.65	1
MSB:Bird:32923	168095	16	Oct	935	Lima	−12.03	−76.65	1
MSB:Bird:32943	168115	18	Oct	352	Lima	−12.01	−76.92	1
MSB:Bird:32950	168122	18	Oct	352	Lima	−12.01	−76.92	1
MSB:Bird:32966	168138	18	Oct	352	Lima	−12.01	−76.92	1
MSB:Bird:32967	168139	18	Oct	352	Lima	−12.01	−76.92	1
MSB:Bird:32969	168141	18	Oct	352	Lima	−12.01	−76.92	1
MSB:Bird:32982	168154	19	Oct	352	Lima	−12.01	−76.92	1
MSB:Bird:32988	168160	19	Oct	352	Lima	−12.01	−76.92	1
MSB:Bird:32991	168163	19	Oct	352	Lima	−12.01	−76.92	1
MSB:Bird:33001	168173	19	Oct	352	Lima	−12.01	−76.92	1
MSB:Bird:33006	168178	19	Oct	352	Lima	−12.01	−76.92	1
MSB:Bird:33008	168180	19	Oct	352	Lima	−12.01	−76.92	1
MSB:Bird:33310	168529	4	Sep	4,056	Lima	−11.77	−76.53	1
MSB:Bird:33329	168548	6	Sep	3,910	Lima	−11.76	−76.54	1
MSB:Bird:33351	168570	9	Sep	3,907	Lima	−11.77	−76.53	1
MSB:Bird:33370	168589	12	Sep	3,905	Lima	−11.77	−76.53	1
MSB:Bird:33416	168635	17	Sep	4,056	Lima	−11.77	−76.53	1
MSB:Bird:34736	171462	3	Jul	309	La Libertad	−8.39	−78.65	1
MSB:Bird:34739	171465	3	Jul	309	La Libertad	−8.39	−78.65	1
MSB:Bird:34763	171489	4	Jul	309	La Libertad	−8.39	−78.65	1
MSB:Bird:34830	171556	8	Jul	2,972	Ancash	−8.75	−78.05	1
MSB:Bird:34832	171558	8	Jul	2,972	Ancash	−8.75	−78.05	1
MSB:Bird:34892	171618	11	Jul	2,972	Ancash	−8.75	−78.05	1
MSB:Bird:34903	171629	12	Jul	357	La Libertad	−8.69	−78.38	1
MSB:Bird:34907	171633	13	Jul	357	La Libertad	−8.69	−78.38	1
MSB:Bird:34916	171642	13	Jul	357	La Libertad	−8.69	−78.38	1
MSB:Bird:34920	171646	14	Jul	357	La Libertad	−8.69	−78.38	1
MSB:Bird:34921	171647	14	Jul	357	La Libertad	−8.69	−78.38	1
MSB:Bird:34953	171679	16	Jul	3,439	Ancash	−9.34	−77.51	1
MSB:Bird:34965	171691	17	Jul	3,439	Ancash	−9.34	−77.51	1
MSB:Bird:34966	171692	17	Jul	3,439	Ancash	−9.34	−77.51	1
MSB:Bird:34967	171693	17	Jul	3,439	Ancash	−9.34	−77.51	1
MSB:Bird:35007	171733	21	Jul	3,714	Ancash	−9.1	−77.87	1
MSB:Bird:35018	171744	21	Jul	3,714	Ancash	−9.1	−77.87	1
MSB:Bird:35538	172264	8	Aug	3,200	Arequipa	−15.81	−72.67	1
MSB:Bird:36014	173845	18	May	3,740	Ancash	−8.74	−78.04	1
MSB:Bird:36049	173880	23	May	3,740	Ancash	−9.02	−77.54	1

Table S1. Cont.

Catalog no. with embedded web link	NK	Day	Month	Elevation, m	Department	Latitude	Longitude	mtDNA clade
MSB:Bird:36081	173912	30	May	3,350	Ancash	−8.84	−77.93	1
MSB:Bird:36568	175520	22	Oct	4,000	Lima	−11.77	−76.53	1
MSB:Bird:36573	175525	24	Oct	4,116	Lima	−11.77	−76.53	1
MSB:Bird:36574	175526	24	Oct	4,123	Lima	−11.77	−76.53	1
MSB:Bird:32351	167523	15	Jul	2,052	Amazonas	−6.1	−78.34	2
MSB:Bird:32619	167791	22	Jul	2,066	Amazonas	−6.1	−78.34	2
MSB:Bird:32855	168027	28	Jul	2,073	Amazonas	−6.1	−78.34	2
MSB:Bird:32862	168034	29	Jul	2,073	Amazonas	−6.1	−78.34	2
MSB:Bird:33894	169120	26	Dec	143	Lambayeque	−5.9	−79.79	2
MSB:Bird:34057	169283	22	Dec	2,215	Piura	−5.84	−79.51	2
MSB:Bird:34076	169302	23	Dec	2,215	Piura	−5.84	−79.51	2
MSB:Bird:34773	171499	4	Jul	309	La Libertad	−8.39	−78.65	2
MSB:Bird:34902	171628	12	Jul	357	La Libertad	−8.69	−78.38	2
MSB:Bird:27066	159722	26	Nov	3,120	Cusco	−13.63	−71.72	3
MSB:Bird:27076	159732	27	Nov	3,120	Cusco	−13.63	−71.72	3
MSB:Bird:27083	159740	28	Nov	3,120	Cusco	−13.63	−71.72	3
MSB:Bird:27131	159789	4	Dec	4,300	Cusco	−13.2	−72.16	3
MSB:Bird:27132	159790	4	Dec	4,300	Cusco	−13.2	−72.16	3
MSB:Bird:27154	159814	8	Dec	3,380	Cusco	−13.25	−72.17	3
MSB:Bird:27174	159834	9	Dec	3,380	Cusco	−13.25	−72.17	3
MSB:Bird:27179	159840	9	Dec	3,380	Cusco	−13.25	−72.17	3
MSB:Bird:27181	159842	10	Dec	3,380	Cusco	−13.25	−72.17	3
MSB:Bird:27203	159868	12	Dec	3,380	Cusco	−13.25	−72.17	3
MSB:Bird:27218	159887	13	Dec	3,380	Cusco	−13.25	−72.17	3
MSB:Bird:31835	163507	18	Jun	3,710	Junin	−11.98	−74.93	3
MSB:Bird:33119	168338	12	Mar	4,030	Cusco	−13.19	−72.23	3
MSB:Bird:33650	168876	4	Dec	3,573	Apurimac	−14.41	−73.09	3
MSB:Bird:33659	168885	5	Dec	3,548	Apurimac	−14.41	−73.09	3
MSB:Bird:34084	169310	9	Jan	4,369	Apurimac	−14.06	−73.01	3
MSB:Bird:34085	169311	9	Jan	4,454	Apurimac	−14.06	−73	3
MSB:Bird:34089	169315	9	Jan	4,375	Apurimac	−14.06	−73.01	3
MSB:Bird:34106	169332	9	Jan	4,384	Apurimac	−14.06	−73.01	3
MSB:Bird:34109	169335	10	Jan	4,375	Apurimac	−14.06	−73.01	3
MSB:Bird:34114	169340	10	Jan	4,401	Apurimac	−14.06	−73.01	3
MSB:Bird:34202	169428	14	Jan	4,363	Apurimac	−14.06	−73	3
MSB:Bird:34295	171021	30	May	1,500	Cusco	−12.65	−72.32	3
MSB:Bird:34359	171085	3	Jun	1,500	Cusco	−12.65	−72.32	3
MSB:Bird:35522	172248	8	Aug	3,200	Arequipa	−15.81	−72.67	3
MSB:Bird:35700	172426	28	Sep	2,671	Apurimac	−14.17	−73.32	3
MSB:Bird:35822	172637	5	Aug	3,201	Cusco	−13.08	−72.37	3
MSB:Bird:35907	172722	21	Sep	2,672	Apurimac	−14.17	−73.32	3
MSB:Bird:35908	172723	21	Sep	2,671	Apurimac	−14.17	−73.32	3
MSB:Bird:28029	162535	20	Jun	322	San Martín	−6.65	−76.07	4
MSB:Bird:33581	168807	19	Nov	2,500	Cusco	−13.56	−70.88	4
MSB:Bird:36130	173961	13	Jun	1,673	San Martin	−7.42	−76.29	4
MSB:Bird:36909	176089	23	Jun	292	Madre de Dios	−11.71	−69.21	4
MSB:Bird:37014	176194	26	Jun	297	Madre de Dios	−11.71	−69.21	4
MSB:Bird:37084	176264	28	Jun	297	Madre de Dios	−11.71	−69.21	4
MSB:Bird:37149	176329	30	Jun	290	Madre de Dios	−11.71	−69.21	4
MSB:Bird:37202	176382	1	Jul	297	Madre de Dios	−11.71	−69.21	4
MSB:Bird:37318	176498	4	Jul	297	Madre de Dios	−11.71	−69.21	4
MSB:Bird:37341	176521	5	Jul	297	Madre de Dios	−11.71	−69.21	4
MSB:Bird:33720	168946	15	Dec	133	Lambayeque	−5.9	−79.79	5
MSB:Bird:33725	168951	15	Dec	133	Lambayeque	−5.9	−79.79	5
MSB:Bird:33758	168984	16	Dec	129	Lambayeque	−5.9	−79.78	5
MSB:Bird:33778	169004	18	Dec	133	Lambayeque	−5.9	−79.79	5
MSB:Bird:33779	169005	18	Dec	133	Lambayeque	−5.9	−79.79	5
MSB:Bird:33844	169070	21	Dec	133	Lambayeque	−5.9	−79.79	5
MSB:Bird:33889	169115	25	Dec	143	Lambayeque	−5.9	−79.79	5
MSB:Bird:34698	171424	2	Jul	309	La Libertad	−8.39	−78.65	5
MSB:Bird:34699	171425	2	Jul	309	La Libertad	−8.39	−78.65	5

Table S1. Cont.

Catalog no. with embedded web link	NK	Day	Month	Elevation, m	Department	Latitude	Longitude	mtDNA clade
MSB:Bird:34893	171619	11	Jul	2,972	Ancash	−8.75	−78.05	5
MSB:Bird:35250	171976	13	Jul	2,500	Cajamarca	−7.4	−78.78	5
MSB:Bird:35330	172056	17	Jul	2,550	Cajamarca	−7.4	−78.78	5
MSB:Bird:35393	172119	21	Jul	2,550	Cajamarca	−7.4	−78.78	5
MSB:Bird:35402	172128	22	Jul	2,550	Cajamarca	−7.4	−78.78	5
MSB:Bird:35035	171761	30	Jul	740	Tacna	−17.56	−70.67	6
MSB:Bird:35043	171769	31	Jul	740	Tacna	−17.56	−70.67	6
MSB:Bird:35046	171772	31	Jul	740	Tacna	−17.56	−70.67	6
MSB:Bird:35047	171773	31	Jul	740	Tacna	−17.56	−70.67	6
MSB:Bird:35057	171783	1	Aug	740	Tacna	−17.56	−70.67	6
MSB:Bird:35442	172168	1	Aug	2,200	Tacna	−17.39	−70.35	6
MSB:Bird:35476	172202	3	Aug	2,975	Tacna	−17.32	−70.25	6
MSB:Bird:35491	172217	4	Aug	2,975	Tacna	−17.32	−70.25	6
MSB:Bird:35493	172219	4	Aug	2,975	Tacna	−17.32	−70.25	6
MSB:Bird:35507	172233	4	Aug	2,975	Tacna	−17.32	−70.25	6
MSB:Bird:35512	172238	5	Aug	2,975	Tacna	−17.32	−70.25	6
MSB:Bird:31626	163191	29	Jan	2,798	Huánuco	−9.73	−76.11	7
MSB:Bird:35697	172423	27	Nov	—	Ancash	—	—	7

Table S2. Summary of nucleotide polymorphism at adult-expressed globin genes of high- and low-altitude house wrens

Gene	Sample	N^a	S^b	h	H_d	π (Sil)	θ_W/bp (Sil)	Tajima's D	$4Nc$
α^A-globin (671 bp)	High altitude	44	7	5	0.385	0.0011	0.0019	−0.9087	0.0000
	Low altitude	66	12	9	0.724	0.0019	0.0047	−1.5318	0.0033
	Total	110	13	10	0.626	0.0016	0.0048	−1.6378	0.0004
α^D-globin (345 bp)	High altitude	48	11	16	0.850	0.0126	0.0162	−0.6671	0.3953
	Low altitude	64	8	13	0.694	0.0089	0.0101	−0.3082	0.0241
	Total	112	13	22	0.769	0.0105	0.0147	−0.7543	0.0823
β^A-globin (1,297 bp)	High altitude	46	35	35	0.989	0.0049	0.0078	−1.2418	0.0818
	Low altitude	58	41	44	0.984	0.0052	0.0089	−1.3942	0.1258
	Total	104	58	72	0.991	0.0053	0.0111	−1.6527	0.1096

Estimates of π, θ_W, and Tajima's D are based on variation at silent sites. h, no. haplotypes; H_d, haplotype diversity; N, no. sampled chromosomes; S, no. segregating sites.

Table S3. Nucleotide differentiation of globin genes between high- and low-altitude populations of Andean house wrens (<1,000 and >3,000 m above sea level, respectively)

Gene	L, bp	N	S	F_{ST}
α^D-globin	345	112	13	0.006
α^A-globin	671	110	13	0.023
ρ-globin	595	100	28	0.054
β^H-globin	617	82	36	0.094
β^A-globin	1,297	104	58	0.133
myoglobin	426	110	19	0.008

Estimates of F_{ST} are based on sets of specimens comprising the central Peru sample (see text for details). The α-type globin genes (α^A and α^D), the β-type globin genes (ρ, β^H, and β^A), and myoglobin are located on different chromosomes. L, length of sequenced fragment; n, number of sampled chromosomes; S, number of segregating sites.

Table S4. O_2 affinities (P_{50}, torr; mean ± SEM) and cooperativity coefficients (n_{50}) for native HbA and HbD isoforms of high- and low-altitude house wrens

Property	Lowland HbA (β55Val)	Highland HbA (β55Ile)	Lowland HbD (β55Val)	Highland HbD (β55Ile)
P_{50}, torr				
Stripped	2.80 ± 0.25	2.47 ± 0.07	1.58 ± 0.03	1.59 ± 0.03
+KCl	4.57 ± 0.01	2.96 ± 0.20	2.67 ± 0.09	2.47 ± 0.04
+IHP	33.90 ± 1.61	21.39 ± 0.32	22.60 ± 0.74	17.54 ± 0.31
KCl + IHP	25.88 ± 1.22	17.07 ± 0.79	16.29 ± 0.19	13.45 ± 0.29
n_{50}				
Stripped	1.48 ± 0.15	1.53 ± 0.04	1.47 ± 0.07	1.36 ± 0.10
+KCl	1.91 ± 0.07	1.36 ± 0.09	1.92 ± 0.11	1.81 ± 0.02
+IHP	1.98 ± 0.25	1.37 ± 0.14	2.39 ± 0.06	2.22 ± 0.14
KCl + IHP	2.11 ± 0.13	1.36 ± 0.01	2.36 ± 0.12	2.28 ± 0.10

O_2 equilibria of purified Hb solutions were measured in 0.1 M Hepes buffer at pH 7.40, 37 °C (heme, 0.3 mM). Measurements were conducted in the absence of anionic effectors (stripped), in the presence of 0.1 M KCl or IHP (IHP/Hb tetramer ratio = 2.0), and in the presence of both effectors, as indicated. [Heme], 0.3 mM. For each population sample, the predominant allelic state of site β55 is given in parentheses.

Table S5. O_2 affinities (P_{50}, torr; mean ± SEM) and cooperativity coefficients (n_{50}) for purified house wren rHbs measured in 0.1 M Hepes buffer at pH 7.40, 37 °C

Property	β55Val-β80Ser (LA)	β55Ile-β80Ser (HA)	β55Val-β80Gly	β55Ile-β80Gly
P_{50}, torr				
Stripped	3.21 ± 0.04	3.17 ± 0.07	2.74 ± 0.02	3.40 ± 0.08
+KCl	5.07 ± 0.06	4.03 ± 0.01	4.21 ± 0.09	4.17 ± 0.10
+IHP	30.82 ± 5.09	26.23 ± 4.93	27.87 ± 3.64	25.23 ± 1.05
KCl + IHP	23.65 ± 2.00	17.86 ± 1.80	18.53 ± 1.61	16.88 ± 0.85
n_{50}				
Stripped	1.61 ± 0.03	1.49 ± 0.05	1.52 ± 0.01	1.66 ± 0.06
+KCl	1.76 ± 0.04	1.77 ± 0.01	1.82 ± 0.06	1.46 ± 0.05
+IHP	1.00 ± 0.13	0.85 ± 0.11	1.17 ± 0.14	1.25 ± 0.05
KCl + IHP	1.30 ± 0.13	0.92 ± 0.09	1.30 ± 0.13	1.16 ± 0.06

Measurements were conducted in the absence of anionic effectors (stripped), in the presence of 0.1 M KCl or IHP (IHP/Hb tetramer ratio = 2.0), and in the presence of both effectors, as indicated. [Heme], 0.3 mM. "HA" and "LA" notations refer to two-site genotypes that are characteristic of high- and low-altitude house wrens, respectively.

Table S6. Single-residue frustration indices for two mutant sites in house wren HbA

	Single-residue frustration index, arbitrary units	
Two-site genotype	β55	β80
β55Val-β80Ser	1.5	0.9
β55Ile-β80Ser	2.0	1.0
β55Val-β80Gly	1.5	0.2
β55Ile-β80Gly	2.1	0.3

At β55 (the sixth residue position of the D helix), the replacement of Val with the more bulky Ile at the $\alpha_1\beta_1$ intersubunit interface induces conformational strain on the β-chain D helix. This is reflected by the fact that β55Ile has a uniformly higher frustration index relative to Val at the same residue position. At β80, the hydroxyl side chain of Ser forms a helix-capping hydrogen bond with β83Asn, the penultimate C-terminal residue of the EF interhelical loop. The helix-capping hydrogen bond between β80Ser and β83Asn confers added rigidity to the E helix, and is reflected by the consistently higher frustration index for β80Ser relative to Gly at the same position.

Supporting Information

Galen et al. 10.1073/pnas.1507300112

SI Methods

Sample Collection. All birds were live-trapped in mist nets and were sacrificed in accordance with protocols approved by the University of New Mexico Institutional Care and Use Committee (Protocol 08UNM033-TR-100117; Animal Welfare Assurance number A4023-01). All collections were authorized by permits issued by management authorities of Peru (004-2007-INRENA-IFFS-DCB, 135-2009-AG-DGFFS-DGEFFS, 0377-2010-AG-DGFFS-DGEFFS, 0199-2012-AG-DGFFS-DGEFFS, and 006-2013-MINAGRI-DGFFS/DGEFFS).

For each of the 140 house wren specimens, we collected 20–60 μL of whole blood from the brachial or ulnar vein using heparinized microcapillary tubes. Red blood cells were separated from the plasma fraction by centrifugation, and the packed red cells were flash-frozen in liquid nitrogen. We collected liver and pectoral muscle from each specimen as sources of genomic DNA and globin mRNA, respectively. Muscle samples were flash-frozen or preserved using RNAlater. All tissue and blood samples were subsequently stored at −80 °C.

Tandem Mass Spectrometry. Database searches of MS/MS spectra were performed using Mascot (Matrix Science; version 1.9.0). Specifically, peptide mass fingerprints derived from the MS/MS analysis were used to query a custom database of avian α- and β-type globin sequences. These amino acid sequences were derived from conceptual translations of the adult-expressed α^A-, α^D-, and β^A-globin genes of *T. aedon*, in addition to the full complement of embryonic and adult α- and β-type globin genes that have been annotated in the genome assemblies of other birds (22–24, 27, 56). We identified all significant protein hits that matched more than one peptide with $P < 0.05$. After separating the HbA and HbD isoforms by native gel IEF and identifying each band on the gel by MS/MS, the relative abundance of the different isoforms was quantified densitometrically.

PCR, Cloning, and Sanger Sequencing. We extracted genomic DNA from frozen tissues of each of the 140 house wren specimens using the DNeasy Blood and Tissue Kit (Qiagen). We used the PCR to amplify six autosomal loci, including full-length coding sequences of the adult-expressed α- and β-type globin genes (α^A-, α^D-, and β^A-globin), intron 2 sequences of ρ-globin and β^H-globin (β-type globin genes that are located just upstream of β^A-globin), and intron 2 of the unlinked myoglobin gene. Negative controls were included in each PCR to control for contamination. All PCR amplicons were purified using ExoSap-IT (USB) and were sequenced in both directions using dye terminator cycle-sequencing (BigDye; ABI) on an ABI 3130 automated sequencer (Applied Biosystems).

For the 14 specimens used in the experimental analyses of Hb function, we extracted RNA from pectoral muscle tissue using the RNeasy kit (Qiagen) and we amplified full-length cDNAs of the α^A, α^D-, and β^A-globin genes using a OneStep RT-PCR kit (Qiagen). We designed paralog-specific primers using 5′- and 3′-UTR sequences from passerine species, as described previously (23). We cloned RT-PCR products using the TOPO TA Cloning Kit (Life Technologies), and we sequenced at least five clones per gene to recover both alleles of each globin gene. This enabled us to determine full diploid genotypes for each of the three adult-expressed globin genes in each specimen.

Population Genetic Analysis. We computed summary statistics of nucleotide polymorphism for each of the adult-expressed globin genes (α^A-, α^D-, and β^A-globin). As a measure of nucleotide variation, we calculated nucleotide diversity, π, and Watterson's θ_W, an estimator of the population mutation rate (=$4N\mu$, where N is the effective population size and μ is the mutation rate per nucleotide). We calculated Tajima's D to characterize the distribution of allele frequencies at silent sites and we calculated Hudson's (57) estimator of the population recombination rate, $4Nc$, where c is the rate of crossing over between adjacent nucleotides. To test whether measured values of Tajima's D deviated from neutral-equilibrium expectations, we obtained critical values for each statistic by conducting 10,000 coalescent simulations (no recombination) that were conditioned on the observed number of segregating sites.

Genome-Wide Survey of Nucleotide Differentiation Using a Genotyping-by-Sequencing Approach. To more broadly survey patterns of genomic differentiation between high- and low-elevation populations, we produced multiplexed, reduced-representation Illumina libraries following Parchman et al. (58). Briefly, we digested genomic DNA samples for a total of 28 individuals (14 from high elevation and 14 from low elevation; Table S1) with two restriction endonucleases (EcoRI and Mse1). We then ligated double-stranded adaptor oligonucleotides that contained Illumina sequencing binding sites and a unique 8- to 10-bp barcode for individual identification, and PCR amplified these adaptor-ligated fragments. Details on the adaptor sequences as well as the digestion and PCR conditions can be found in the study by Parchman et al. (58). We pooled the barcoded amplicons from each individual in equimolar concentrations, and electrophoresed them on 2.5% agarose gel for size selection. Fragments that were between 350 and 500 bp in length were excised from the gel and purified using a QIAquick Gel Extraction Kit (Qiagen). The pooled library was sequenced in a single lane on the Illumina HiSEq 1000 platform as 100-nt single-end reads at the Keck Center for Comparative and Functional Genomics at the University of Illinois, Urbana–Champaign.

We parsed the resulting reads by individual barcodes and trimmed adaptor sequences and low-quality bases using custom Perl scripts, resulting in a final mean read length of 87 nt. To limit our analysis to putative protein-coding genes, we mapped individual *T. aedon* reads to the published transcriptome of a closely related passerine, *Zontrichia leucophrys* (59), using the *sensitive-local* settings in Bowtie2 (60). Transcript-aligned reads were then processed using the program STACKS (61) to identify single-nucleotide polymorphisms (SNPs) in reads that mapped to known transcripts using the following input parameters for pstacks: - m3, –model_type snp, –alpha 0.05. All 28 individuals were included when compiling the SNP catalog in cstacks. Downstream population genetic analysis were restricted to loci that were genotyped in at least 10 individuals per population with a minimum sequencing depth of 5 reads per locus per individual and a minor allele frequency of 0.05, resulting in a final dataset of 1,272 unique loci. We calculated locus-specific F_{ST} values using the program POPULATIONS implemented in STACKS (61).

Protein Purification and in Vitro Analysis of Hb Function. We purified HbA and HbD variants from pooled hemolysates from seven highland specimens and seven lowland specimens. There was a nearly fixed difference between the two samples at β55, with Ile and Val alleles predominating in the highland and lowland specimens, respectively, but there was also a low level of amino acid heterogeneity at site β80: a derived Gly allele was present at

frequencies of 0.36 and 0.07 in the samples of highland and lowland specimens, respectively (n = 14 alleles in each sample).

Using purified Hb solutions (0.3 mM heme) that were stripped of organic phosphates and other allosteric effectors, we measured O_2 equilibrium curves at 37 °C, 0.1 M Hepes, pH 7.4, in the absence ("stripped") and presence of 0.1 M KCl, IHP (at twofold molar excess over tetrameric Hb), and in the simultaneous presence of KCl and IHP. We measured O_2 equilibria of 3-μL thin-film samples in a modified diffusion chamber where absorption at 436 nm was monitored during stepwise changes in equilibration gas mixtures generated by precision Wösthoff gas-mixing pumps. We estimated values of P_{50} and n_{50} (Hill's cooperativity coefficient at half-saturation) by fitting the Hill equation $Y = PO_2^n/(P_{50}^n + PO_2^n)$ to the experimental O_2 saturation data by means of nonlinear regression (Y = fractional O_2 saturation; n, cooperativity coefficient) (22, 62–64). The model fitting was based on five to eight equilibration steps between 30% and 70% oxygenation. Free Cl^- concentrations were measured with a model 926S Mark II chloride analyzer (Sherwood Scientific Ltd.).

Expression and Purification of Recombinant Hbs. Recombinant Hb expression was carried out in the JM109 (DE3) *E. coli* strain. Bacterial cells were selected in LB agar with dual antibiotics (ampicillin and kanamycin) to ensure that transformants received both pGM and pCO-MAP plasmids for expression. The expression of each rHb mutant was carried out in 1.5 L of TB medium. Bacterial cells were grown in 37 °C in an orbital shaker at 200 rpm until absorbance values reached 0.6–0.8 at 600 nm. The bacterial cultures were induced by 0.2 mM isopropyl β-D-1-thiogalactopyranoside and were then supplemented with hemin (50 μg/mL) and glucose (20 g/L). The bacterial culture conditions and the protocol for preparing cell lysates are described in the study by Natarajan et al. (53).

We purified each rHb sample by means of two step ion-exchange chromatography as described previously (32, 37, 38, 40, 53). Samples were passed through a cation-exchange column (HiTrap SP-Sepharose; GE Healthcare; 17-1152-01) followed by equilibration with 20 mM Tris buffer (0.5 mM EDTA, 0.5 mM DTT, pH 6.0) and elution using a linear gradient of 0–0.5 M NaCl. The eluted fractions were passed through an anion-exchange column (HiTrap Q-Sepharose; GE Healthcare; 17-1153-01), followed by equilibration with 20 mM Tris buffer (0.5 mM EDTA, 0.5 mM DTT, pH 8.5), and elution using a linear gradient of 0–0.5 M NaCl. The samples were desalted by dialysis against 10 mM Hepes buffer (pH 7.6) at 4 °C. The eluted fractions of each rHb sample were concentrated by using centrifugal filtrate. The purified rHb samples were analyzed by SDS-polyacrylamide gel electrophoresis and isoelectrofocusing (IEF). After preparing rHb samples as oxyHb, deoxyHb, and carbonmonoxy derivatives, we measured absorbance at 450–600 nm to confirm that the absorbance maxima match those of the native HbA samples.

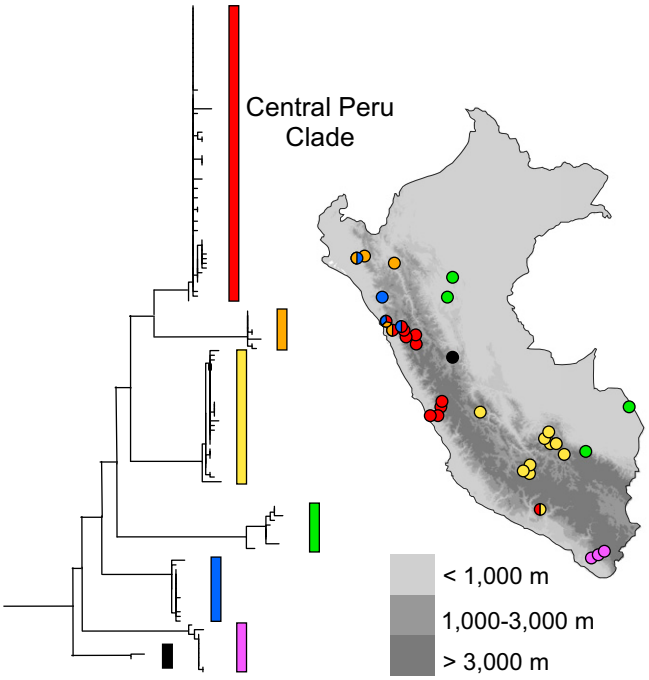

Fig. S1. Phylogeographic population structure of house wrens sampled from throughout Peru. The tree (*Left*) shows relationships among well-defined mtDNA clades. In the map (*Right*), color coding of symbols shows the proportional representation of different mtDNA clades in samples of house wren specimens from each locality. Specimens comprising the "central Peru clade" served as the focus for the elevational survey of genomic polymorphism, as described in the main text.

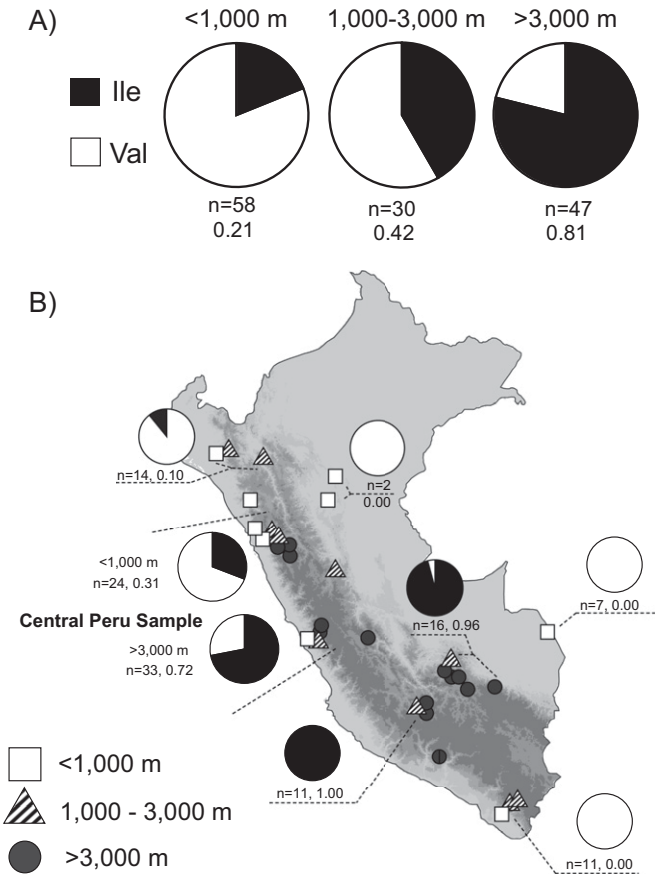

Fig. S2. The β55(Val/Ile) polymorphism exhibits a striking altitudinal pattern of allele frequency variation in natural populations of Peruvian house wrens. (*A*) The β55Ile allele predominates at high altitude, and the Val allele predominates at lower altitudes. (*B*) Variation in frequency of the derived β55Ile allele across Peru. The central Peru sample comprises a phylogeographically defined set of specimens that served as the focus for the elevational survey of genomic polymorphism.

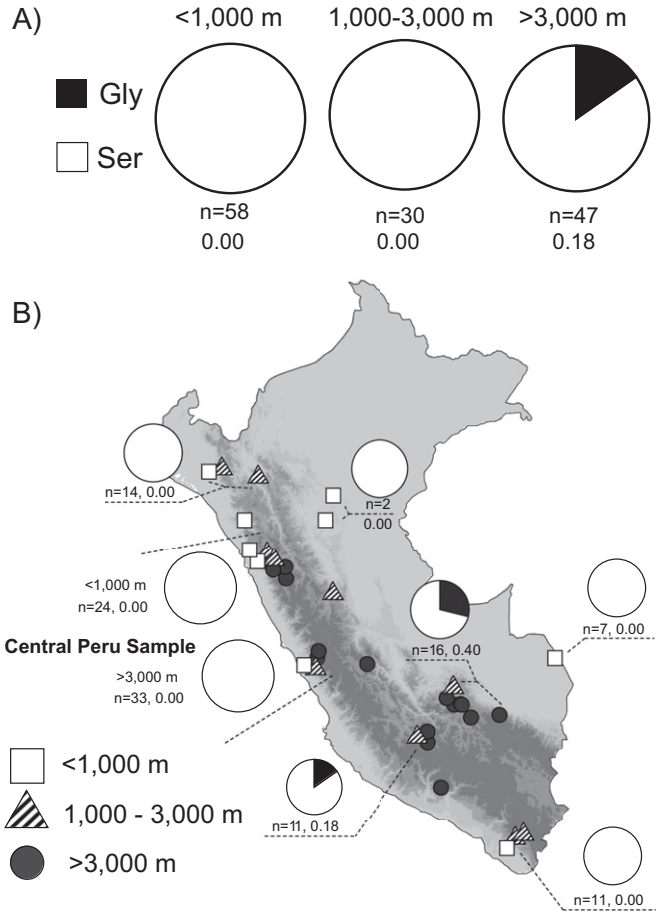

Fig. S3. In addition to the β55(Val/Ile) polymorphism, β80 is one of the only other amino acid sites that harbors segregating variation in natural populations of Peruvian house wrens. However, the ancestral Ser allele predominates in population samples from every elevational zone. (*A*) The derived β80Gly allele is present at moderate frequencies in population samples from the highlands of southern Peru. (*B*) Variation in frequency of the derived β80Gly allele across Peru. The central Peru sample comprises a phylogeographically defined set of specimens that served as the focus for the elevational survey of genomic polymorphism.

Table S1. House wren samples used in this study with ARCTOS Museum of Southwestern Biology catalog web link, sampling details, and mtDNA clade from Galen and Witt (20)

Catalog no. with embedded web link	NK	Day	Month	Elevation, m	Department	Latitude	Longitude	mtDNA clade
MSB:Bird:27052	159705	30	Oct	3,040	Lima	−11.76	−76.58	1
MSB:Bird:27596	162008	3	Jun	366	Lima	−12.01	−76.92	1
MSB:Bird:27606	162022	3	Jun	366	Lima	−12.01	−76.92	1
MSB:Bird:27609	162025	3	Jun	366	Lima	−12.01	−76.92	1
MSB:Bird:31418	162982	8	Jan	372	Lima	−12	−76.92	1
MSB:Bird:31425	162989	8	Jan	351	Lima	−12	−76.92	1
MSB:Bird:31433	162997	8	Jan	372	Lima	−12	−76.92	1
MSB:Bird:31450	163014	9	Jan	352	Lima	−12.01	−76.92	1
MSB:Bird:31454	163018	9	Jan	352	Lima	−12.01	−76.92	1
MSB:Bird:31456	163020	9	Jan	352	Lima	−12.01	−76.92	1
MSB:Bird:31459	163023	9	Jan	352	Lima	−12.01	−76.92	1
MSB:Bird:31469	163033	12	Jan	3,967	Lima	−11.63	−76.43	1
MSB:Bird:31482	163046	12	Jan	3,959	Lima	−11.63	−76.43	1
MSB:Bird:31489	163053	13	Jan	3,973	Lima	−11.63	−76.43	1
MSB:Bird:31498	163062	13	Jan	3,981	Lima	−11.63	−76.43	1
MSB:Bird:31503	163067	14	Jan	3,967	Lima	−11.63	−76.43	1
MSB:Bird:31739	163411	7	May	3,750	Lima	−11.76	−76.55	1
MSB:Bird:31756	163428	21	May	2,400	Lima	−11.74	−76.61	1
MSB:Bird:31766	163438	24	May	2,400	Lima	−11.74	−76.61	1
MSB:Bird:31767	163439	24	May	2,400	Lima	−11.74	−76.61	1
MSB:Bird:32902	168074	15	Oct	935	Lima	−12.03	−76.65	1
MSB:Bird:32909	168081	15	Oct	935	Lima	−12.03	−76.65	1
MSB:Bird:32910	168082	15	Oct	935	Lima	−12.03	−76.65	1
MSB:Bird:32922	168094	16	Oct	935	Lima	−12.03	−76.65	1
MSB:Bird:32923	168095	16	Oct	935	Lima	−12.03	−76.65	1
MSB:Bird:32943	168115	18	Oct	352	Lima	−12.01	−76.92	1
MSB:Bird:32950	168122	18	Oct	352	Lima	−12.01	−76.92	1
MSB:Bird:32966	168138	18	Oct	352	Lima	−12.01	−76.92	1
MSB:Bird:32967	168139	18	Oct	352	Lima	−12.01	−76.92	1
MSB:Bird:32969	168141	18	Oct	352	Lima	−12.01	−76.92	1
MSB:Bird:32982	168154	19	Oct	352	Lima	−12.01	−76.92	1
MSB:Bird:32988	168160	19	Oct	352	Lima	−12.01	−76.92	1
MSB:Bird:32991	168163	19	Oct	352	Lima	−12.01	−76.92	1
MSB:Bird:33001	168173	19	Oct	352	Lima	−12.01	−76.92	1
MSB:Bird:33006	168178	19	Oct	352	Lima	−12.01	−76.92	1
MSB:Bird:33008	168180	19	Oct	352	Lima	−12.01	−76.92	1
MSB:Bird:33310	168529	4	Sep	4,056	Lima	−11.77	−76.53	1
MSB:Bird:33329	168548	6	Sep	3,910	Lima	−11.76	−76.54	1
MSB:Bird:33351	168570	9	Sep	3,907	Lima	−11.77	−76.53	1
MSB:Bird:33370	168589	12	Sep	3,905	Lima	−11.77	−76.53	1
MSB:Bird:33416	168635	17	Sep	4,056	Lima	−11.77	−76.53	1
MSB:Bird:34736	171462	3	Jul	309	La Libertad	−8.39	−78.65	1
MSB:Bird:34739	171465	3	Jul	309	La Libertad	−8.39	−78.65	1
MSB:Bird:34763	171489	4	Jul	309	La Libertad	−8.39	−78.65	1
MSB:Bird:34830	171556	8	Jul	2,972	Ancash	−8.75	−78.05	1
MSB:Bird:34832	171558	8	Jul	2,972	Ancash	−8.75	−78.05	1
MSB:Bird:34892	171618	11	Jul	2,972	Ancash	−8.75	−78.05	1
MSB:Bird:34903	171629	12	Jul	357	La Libertad	−8.69	−78.38	1
MSB:Bird:34907	171633	13	Jul	357	La Libertad	−8.69	−78.38	1
MSB:Bird:34916	171642	13	Jul	357	La Libertad	−8.69	−78.38	1
MSB:Bird:34920	171646	14	Jul	357	La Libertad	−8.69	−78.38	1
MSB:Bird:34921	171647	14	Jul	357	La Libertad	−8.69	−78.38	1
MSB:Bird:34953	171679	16	Jul	3,439	Ancash	−9.34	−77.51	1
MSB:Bird:34965	171691	17	Jul	3,439	Ancash	−9.34	−77.51	1
MSB:Bird:34966	171692	17	Jul	3,439	Ancash	−9.34	−77.51	1
MSB:Bird:34967	171693	17	Jul	3,439	Ancash	−9.34	−77.51	1
MSB:Bird:35007	171733	21	Jul	3,714	Ancash	−9.1	−77.87	1
MSB:Bird:35018	171744	21	Jul	3,714	Ancash	−9.1	−77.87	1
MSB:Bird:35538	172264	8	Aug	3,200	Arequipa	−15.81	−72.67	1
MSB:Bird:36014	173845	18	May	3,740	Ancash	−8.74	−78.04	1
MSB:Bird:36049	173880	23	May	3,740	Ancash	−9.02	−77.54	1

Table S1. Cont.

Catalog no. with embedded web link	NK	Day	Month	Elevation, m	Department	Latitude	Longitude	mtDNA clade
MSB:Bird:36081	173912	30	May	3,350	Ancash	−8.84	−77.93	1
MSB:Bird:36568	175520	22	Oct	4,000	Lima	−11.77	−76.53	1
MSB:Bird:36573	175525	24	Oct	4,116	Lima	−11.77	−76.53	1
MSB:Bird:36574	175526	24	Oct	4,123	Lima	−11.77	−76.53	1
MSB:Bird:32351	167523	15	Jul	2,052	Amazonas	−6.1	−78.34	2
MSB:Bird:32619	167791	22	Jul	2,066	Amazonas	−6.1	−78.34	2
MSB:Bird:32855	168027	28	Jul	2,073	Amazonas	−6.1	−78.34	2
MSB:Bird:32862	168034	29	Jul	2,073	Amazonas	−6.1	−78.34	2
MSB:Bird:33894	169120	26	Dec	143	Lambayeque	−5.9	−79.79	2
MSB:Bird:34057	169283	22	Dec	2,215	Piura	−5.84	−79.51	2
MSB:Bird:34076	169302	23	Dec	2,215	Piura	−5.84	−79.51	2
MSB:Bird:34773	171499	4	Jul	309	La Libertad	−8.39	−78.65	2
MSB:Bird:34902	171628	12	Jul	357	La Libertad	−8.69	−78.38	2
MSB:Bird:27066	159722	26	Nov	3,120	Cusco	−13.63	−71.72	3
MSB:Bird:27076	159732	27	Nov	3,120	Cusco	−13.63	−71.72	3
MSB:Bird:27083	159740	28	Nov	3,120	Cusco	−13.63	−71.72	3
MSB:Bird:27131	159789	4	Dec	4,300	Cusco	−13.2	−72.16	3
MSB:Bird:27132	159790	4	Dec	4,300	Cusco	−13.2	−72.16	3
MSB:Bird:27154	159814	8	Dec	3,380	Cusco	−13.25	−72.17	3
MSB:Bird:27174	159834	9	Dec	3,380	Cusco	−13.25	−72.17	3
MSB:Bird:27179	159840	9	Dec	3,380	Cusco	−13.25	−72.17	3
MSB:Bird:27181	159842	10	Dec	3,380	Cusco	−13.25	−72.17	3
MSB:Bird:27203	159868	12	Dec	3,380	Cusco	−13.25	−72.17	3
MSB:Bird:27218	159887	13	Dec	3,380	Cusco	−13.25	−72.17	3
MSB:Bird:31835	163507	18	Jun	3,710	Junin	−11.98	−74.93	3
MSB:Bird:33119	168338	12	Mar	4,030	Cusco	−13.19	−72.23	3
MSB:Bird:33650	168876	4	Dec	3,573	Apurimac	−14.41	−73.09	3
MSB:Bird:33659	168885	5	Dec	3,548	Apurimac	−14.41	−73.09	3
MSB:Bird:34084	169310	9	Jan	4,369	Apurimac	−14.06	−73.01	3
MSB:Bird:34085	169311	9	Jan	4,454	Apurimac	−14.06	−73	3
MSB:Bird:34089	169315	9	Jan	4,375	Apurimac	−14.06	−73.01	3
MSB:Bird:34106	169332	9	Jan	4,384	Apurimac	−14.06	−73.01	3
MSB:Bird:34109	169335	10	Jan	4,375	Apurimac	−14.06	−73.01	3
MSB:Bird:34114	169340	10	Jan	4,401	Apurimac	−14.06	−73.01	3
MSB:Bird:34202	169428	14	Jan	4,363	Apurimac	−14.06	−73	3
MSB:Bird:34295	171021	30	May	1,500	Cusco	−12.65	−72.32	3
MSB:Bird:34359	171085	3	Jun	1,500	Cusco	−12.65	−72.32	3
MSB:Bird:35522	172248	8	Aug	3,200	Arequipa	−15.81	−72.67	3
MSB:Bird:35700	172426	28	Sep	2,671	Apurimac	−14.17	−73.32	3
MSB:Bird:35822	172637	5	Aug	3,201	Cusco	−13.08	−72.37	3
MSB:Bird:35907	172722	21	Sep	2,672	Apurimac	−14.17	−73.32	3
MSB:Bird:35908	172723	21	Sep	2,671	Apurimac	−14.17	−73.32	3
MSB:Bird:28029	162535	20	Jun	322	San Martín	−6.65	−76.07	4
MSB:Bird:33581	168807	19	Nov	2,500	Cusco	−13.56	−70.88	4
MSB:Bird:36130	173961	13	Jun	1,673	San Martin	−7.42	−76.29	4
MSB:Bird:36909	176089	23	Jun	292	Madre de Dios	−11.71	−69.21	4
MSB:Bird:37014	176194	26	Jun	297	Madre de Dios	−11.71	−69.21	4
MSB:Bird:37084	176264	28	Jun	297	Madre de Dios	−11.71	−69.21	4
MSB:Bird:37149	176329	30	Jun	290	Madre de Dios	−11.71	−69.21	4
MSB:Bird:37202	176382	1	Jul	297	Madre de Dios	−11.71	−69.21	4
MSB:Bird:37318	176498	4	Jul	297	Madre de Dios	−11.71	−69.21	4
MSB:Bird:37341	176521	5	Jul	297	Madre de Dios	−11.71	−69.21	4
MSB:Bird:33720	168946	15	Dec	133	Lambayeque	−5.9	−79.79	5
MSB:Bird:33725	168951	15	Dec	133	Lambayeque	−5.9	−79.79	5
MSB:Bird:33758	168984	16	Dec	129	Lambayeque	−5.9	−79.78	5
MSB:Bird:33778	169004	18	Dec	133	Lambayeque	−5.9	−79.79	5
MSB:Bird:33779	169005	18	Dec	133	Lambayeque	−5.9	−79.79	5
MSB:Bird:33844	169070	21	Dec	133	Lambayeque	−5.9	−79.79	5
MSB:Bird:33889	169115	25	Dec	143	Lambayeque	−5.9	−79.79	5
MSB:Bird:34698	171424	2	Jul	309	La Libertad	−8.39	−78.65	5
MSB:Bird:34699	171425	2	Jul	309	La Libertad	−8.39	−78.65	5

Table S1. Cont.

Catalog no. with embedded web link	NK	Day	Month	Elevation, m	Department	Latitude	Longitude	mtDNA clade
MSB:Bird:34893	171619	11	Jul	2,972	Ancash	−8.75	−78.05	5
MSB:Bird:35250	171976	13	Jul	2,500	Cajamarca	−7.4	−78.78	5
MSB:Bird:35330	172056	17	Jul	2,550	Cajamarca	−7.4	−78.78	5
MSB:Bird:35393	172119	21	Jul	2,550	Cajamarca	−7.4	−78.78	5
MSB:Bird:35402	172128	22	Jul	2,550	Cajamarca	−7.4	−78.78	5
MSB:Bird:35035	171761	30	Jul	740	Tacna	−17.56	−70.67	6
MSB:Bird:35043	171769	31	Jul	740	Tacna	−17.56	−70.67	6
MSB:Bird:35046	171772	31	Jul	740	Tacna	−17.56	−70.67	6
MSB:Bird:35047	171773	31	Jul	740	Tacna	−17.56	−70.67	6
MSB:Bird:35057	171783	1	Aug	740	Tacna	−17.56	−70.67	6
MSB:Bird:35442	172168	1	Aug	2,200	Tacna	−17.39	−70.35	6
MSB:Bird:35476	172202	3	Aug	2,975	Tacna	−17.32	−70.25	6
MSB:Bird:35491	172217	4	Aug	2,975	Tacna	−17.32	−70.25	6
MSB:Bird:35493	172219	4	Aug	2,975	Tacna	−17.32	−70.25	6
MSB:Bird:35507	172233	4	Aug	2,975	Tacna	−17.32	−70.25	6
MSB:Bird:35512	172238	5	Aug	2,975	Tacna	−17.32	−70.25	6
MSB:Bird:31626	163191	29	Jan	2,798	Huánuco	−9.73	−76.11	7
MSB:Bird:35697	172423	27	Nov	—	Ancash	—	—	7

Table S2. Summary of nucleotide polymorphism at adult-expressed globin genes of high- and low-altitude house wrens

Gene	Sample	N^a	S^b	h	H_d	π (Sil)	θ_W/bp (Sil)	Tajima's D	$4Nc$
α^A-globin (671 bp)	High altitude	44	7	5	0.385	0.0011	0.0019	−0.9087	0.0000
	Low altitude	66	12	9	0.724	0.0019	0.0047	−1.5318	0.0033
	Total	110	13	10	0.626	0.0016	0.0048	−1.6378	0.0004
α^D-globin (345 bp)	High altitude	48	11	16	0.850	0.0126	0.0162	−0.6671	0.3953
	Low altitude	64	8	13	0.694	0.0089	0.0101	−0.3082	0.0241
	Total	112	13	22	0.769	0.0105	0.0147	−0.7543	0.0823
β^A-globin (1,297 bp)	High altitude	46	35	35	0.989	0.0049	0.0078	−1.2418	0.0818
	Low altitude	58	41	44	0.984	0.0052	0.0089	−1.3942	0.1258
	Total	104	58	72	0.991	0.0053	0.0111	−1.6527	0.1096

Estimates of π, θ_W, and Tajima's D are based on variation at silent sites. h, no. haplotypes; H_d, haplotype diversity; N, no. sampled chromosomes; S, no. segregating sites.

Table S3. Nucleotide differentiation of globin genes between high- and low-altitude populations of Andean house wrens (<1,000 and >3,000 m above sea level, respectively)

Gene	L, bp	N	S	F_{ST}
α^D-globin	345	112	13	0.006
α^A-globin	671	110	13	0.023
ρ-globin	595	100	28	0.054
β^H-globin	617	82	36	0.094
β^A-globin	1,297	104	58	0.133
myoglobin	426	110	19	0.008

Estimates of F_{ST} are based on sets of specimens comprising the central Peru sample (see text for details). The α-type globin genes (α^A and α^D), the β-type globin genes (ρ, β^H, and β^A), and myoglobin are located on different chromosomes. L, length of sequenced fragment; n, number of sampled chromosomes; S, number of segregating sites.

Table S4. O_2 affinities (P_{50}, torr; mean ± SEM) and cooperativity coefficients (n_{50}) for native HbA and HbD isoforms of high- and low-altitude house wrens

Property	Lowland HbA (β55Val)	Highland HbA (β55Ile)	Lowland HbD (β55Val)	Highland HbD (β55Ile)
P_{50}, torr				
Stripped	2.80 ± 0.25	2.47 ± 0.07	1.58 ± 0.03	1.59 ± 0.03
+KCl	4.57 ± 0.01	2.96 ± 0.20	2.67 ± 0.09	2.47 ± 0.04
+IHP	33.90 ± 1.61	21.39 ± 0.32	22.60 ± 0.74	17.54 ± 0.31
KCl + IHP	25.88 ± 1.22	17.07 ± 0.79	16.29 ± 0.19	13.45 ± 0.29
n_{50}				
Stripped	1.48 ± 0.15	1.53 ± 0.04	1.47 ± 0.07	1.36 ± 0.10
+KCl	1.91 ± 0.07	1.36 ± 0.09	1.92 ± 0.11	1.81 ± 0.02
+IHP	1.98 ± 0.25	1.37 ± 0.14	2.39 ± 0.06	2.22 ± 0.14
KCl + IHP	2.11 ± 0.13	1.36 ± 0.01	2.36 ± 0.12	2.28 ± 0.10

O_2 equilibria of purified Hb solutions were measured in 0.1 M Hepes buffer at pH 7.40, 37 °C (heme, 0.3 mM). Measurements were conducted in the absence of anionic effectors (stripped), in the presence of 0.1 M KCl or IHP (IHP/Hb tetramer ratio = 2.0), and in the presence of both effectors, as indicated. [Heme], 0.3 mM. For each population sample, the predominant allelic state of site β55 is given in parentheses.

Table S5. O_2 affinities (P_{50}, torr; mean ± SEM) and cooperativity coefficients (n_{50}) for purified house wren rHbs measured in 0.1 M Hepes buffer at pH 7.40, 37 °C

Property	β55Val-β80Ser (LA)	β55Ile-β80Ser (HA)	β55Val-β80Gly	β55Ile-β80Gly
P_{50}, torr				
Stripped	3.21 ± 0.04	3.17 ± 0.07	2.74 ± 0.02	3.40 ± 0.08
+KCl	5.07 ± 0.06	4.03 ± 0.01	4.21 ± 0.09	4.17 ± 0.10
+IHP	30.82 ± 5.09	26.23 ± 4.93	27.87 ± 3.64	25.23 ± 1.05
KCl + IHP	23.65 ± 2.00	17.86 ± 1.80	18.53 ± 1.61	16.88 ± 0.85
n_{50}				
Stripped	1.61 ± 0.03	1.49 ± 0.05	1.52 ± 0.01	1.66 ± 0.06
+KCl	1.76 ± 0.04	1.77 ± 0.01	1.82 ± 0.06	1.46 ± 0.05
+IHP	1.00 ± 0.13	0.85 ± 0.11	1.17 ± 0.14	1.25 ± 0.05
KCl + IHP	1.30 ± 0.13	0.92 ± 0.09	1.30 ± 0.13	1.16 ± 0.06

Measurements were conducted in the absence of anionic effectors (stripped), in the presence of 0.1 M KCl or IHP (IHP/Hb tetramer ratio = 2.0), and in the presence of both effectors, as indicated. [Heme], 0.3 mM. "HA" and "LA" notations refer to two-site genotypes that are characteristic of high- and low-altitude house wrens, respectively.

Table S6. Single-residue frustration indices for two mutant sites in house wren HbA

	Single-residue frustration index, arbitrary units	
Two-site genotype	β55	β80
β55Val-β80Ser	1.5	0.9
β55Ile-β80Ser	2.0	1.0
β55Val-β80Gly	1.5	0.2
β55Ile-β80Gly	2.1	0.3

At β55 (the sixth residue position of the D helix), the replacement of Val with the more bulky Ile at the $\alpha_1\beta_1$ intersubunit interface induces conformational strain on the β-chain D helix. This is reflected by the fact that β55Ile has a uniformly higher frustration index relative to Val at the same residue position. At β80, the hydroxyl side chain of Ser forms a helix-capping hydrogen bond with β83Asn, the penultimate C-terminal residue of the EF interhelical loop. The helix-capping hydrogen bond between β80Ser and β83Asn confers added rigidity to the E helix, and is reflected by the consistently higher frustration index for β80Ser relative to Gly at the same position.